SIGNATURES

NEWSLETTER OF INDIAN SOCIETY OF REMOTE SENSING - AHMEDABAD CHAPTER

REMOTE SENSING OF OCEAN: DEVELOPING BLUE ECONOMY

March 2020 Volume 27, Issue 2

March 2020
Volume 27, Issue 2

SIGNATURES

NEWSLETTER OF INDIAN SOCIETY OF REMOTE SENSING - AHMEDABAD CHAPTER

From the Editor's Desk

DR. RASHMI SHARMA

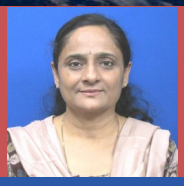

Delighted to be with you once again with this special issue of "Signatures" on "Remote Sensing of Oceans" comprising of articles encompassing various facets of oceans such as biological, physical, coastal, lithosphere etc.

Needless to say, how satellites have changed the whole perspective of observing the oceans. They play a key role in the studies pertaining to integrated oceanography for sustainable development. India's space program has contributed significantly to the understanding of our oceans. It began with Oceansat-1, a dedicated ocean mission with microwave radiometer, MSMR and Ocean colour Monitor which was flown in 1999. This was followed by Oceansat-2 in 2009, SARAL/AltiKa in 2013 and SCATSAT-1 in 2016. We indeed look forward to yet another oceanographic mission, Oceansat-3 to be in space by the end of this year.

Space Applications of Centre (SAC), ISRO, has embarked upon a very ambitious program named SAtellite-based Marine process Understanding, Development, Research and Applications for blue economy (SAMUDRA). Under this program, we have demonstrated the capabilities of different space-borne sensors in addressing the contemporary issues like, coastal hazards and disasters along with applicability of satellite observations for renewable energy, navigation, potential fishing zone etc.

Recently, SAC has brought out an atlas on "Viewing the Oceans from Space", Think Blue – Developing the Nation's Economy" which provides glimpses of our activities (ISBN:978-93-82760-38-2).

The present edition of "Signatures" has been planned in a very meticulous way so as to cover most of the aspects of blue economy. Brief notes covering the topics like plastic pollution, ocean state forecast for safe navigation, ocean energy, marine lithosphere, potential fishing zone, coastal erosion and vulnerability, ocean biology and trajectory prediction of oil-spills have been included in this edition.

Over-exploitation to satisfy our ever-growing greed has led to serious stress on oceans. Together we can create a 'healthy Ocean'. So let's gear up for the World Oceans Day, 8 June 2020. A variety of awareness programmes have been planned globally to protect and preserve the flora and fauna of our oceans (https://worldoceansday.org/).

Inside This Issue

From the Chairman's Desk

DR. RAJ KUMAR

As we all know that Ocean is one of the most important component of the Earth-Atmosphere System, responsible for regulating the Earth's Climate. It is considered as a very valuable natural resource. However, Ocean also plays the role of a "Universal Sewer" wherein all kinds of pollutants drain, which escalates the degradation of ocean resources and habitats. This calls for urgent and structured measures to reverse marine pollution and transit towards a sustainable blue economy by preserving and regrowing ocean resources. ISRS-AC has always been very proactive in encouraging ocean based sustainable development.

This issue of 'Signatures' is one of the important steps towards educating and taking stock of the efforts carried out by Indian Remote Sensing community in the development of the blue economy.

Remote Sensing helps in monitoring and paving the way for healthy coastal and marine ecosystems, renewable energy , sustainable fisheries and mitigating pollution from ocean and land based sources.

We as a responsible Society , ISRS - AC through this issue of 'Signatures' , showcase a miscellany of thought provoking articles tagged to Ocean restoration and sustainable development for Blue Economy. Lets celebrate this issue with the World Oceans Day on 8th June !!

From the Secretary's Desk

DR. A. S. RAJAWAT

I express my delight that the Editorial team of the ISRS-AC Newsletter "Signatures", have brought out this current issue with the theme "Remote Sensing of ocean: Developing Blue Economy ". I feel Ocean in current and near future will play a pivotal role in governing the sustainable economy. ISRS-AC as a remote sensing community is aimed to take up the major task in strengthening the link between researchers and user community.

As can be seen under Section, "Glimpses of ISRS-AC Activities", in this year we have been able to organize many activities jointly along with ISG-AC, INCA-GB, IMSA and IEEE-GRSS, Gujarat Chapter. One of the major endeavours this year was the membership drive, and I am happy to announce that we were able to expand the ISRS-AC family with 13 new life members. Thus, The ISRS-AC continues to be the largest Chapter of the ISRS with 628 members (Fellows: 6, Patron: 7, Sustaining 3, Life: 628).

Also in continuation to our lecture series, an expert lecture entitled, "Vegetation, Agriculture, Data Fusion and Machine Learning", by Dr. Keely Roth, Senior Remote Sensing Scientist and Science Lead for Horticulture on the Geospatial Sciences team of the Climate Corporation at San Francisco CA, USA was held at Nirma University, Ahmedabad on November 13, 2019. This was jointly organized by the Institute of Technology, Nirma University, IEEE-Geoscience and Remote Sensing Society-Gujarat Chapter, IEEE-Student Chapter, Nirma University and ISRS-AC .

As Secretary, ISRS-AC , I also participated in the meeting of the Chapter Secretaries at ISRS HQ, Dehradun held on January 18, 2020. It was an endeavor by ISRS HQ to update all Chapters about various activities of ISRS as well activate and streamline activities of the Chapters. Agenda was primarily on briefing major activities of ISRS and role of Chapters, promoting usage of ISRS website through Chapters, financial guidelines, Chapter elections, organization of regional workshops, support for reviewers of JISRS, increasing membership strength, updating members contact details and discussing suggestions from Chapter representatives to further strengthen activities of ISRS.

I also take this opportunity to welcome the new ISRS-AC executive committee, who will take the baton forward and usher in a new era of scientific community allied sustainable development. I also express my sincere gratitude to all the members of the community who have provided us their unflinching and continued support. Wishing you all a very happy reading. Cheers !!!

GISAT overview

R P SINGH
Head, LHD/GHCAG/EPSA, Space Applications Centre (ISRO), Ahmedabad
rpsingh@sac.isro.gov.in

Introduction

Space technology in the twenty-first century is expected to play an important role in integrating diverse discipline of science to provide solutions related with water security, food security and overall economic security of the nation. Earth observation systems provide an integrated perspective to coupled biogeochemical cycle on earth in different spatial and temporal domains. Despite many earth observation systems exclusive for land (Resourcesat series, ocean (Oceansat series) and atmosphere (INSAT series), there is need to simultaneously measure the state variables of earth surface and atmosphere from single platform. Geo-stationary Imaging Satellite (GISAT) is for integrated observations of Land, Ocean and some of the Atmospheric parameters at high resolution using appropriate wavelength selection. The wide spectral range with multispectral and hyperspectral imaging capability combined with multiple operating modes provides unique opportunity to the user community for applications. Earlier multi spectral CCD sensor onboard INSAT-2E/3A satellite provided useful data covering entire Indian landmass and currently GHRC instrument onboard GSAT-29 instrument is providing multi spectral data from Geostationary platform. The GISAT-1 has advanced capability in terms of optics and coverage of spectral range and resolution. It would provide high resolution imaging through multi spectral sensor as well hyperspectral imaging for scientific explorations.

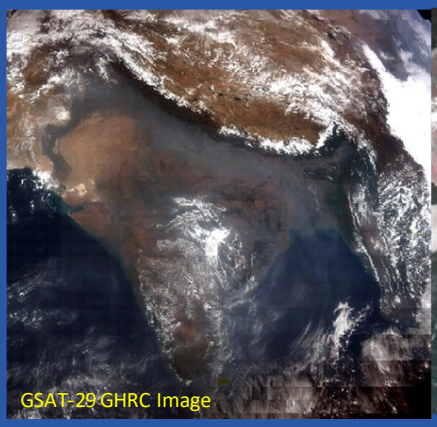
GSAT-29 GHRC Image

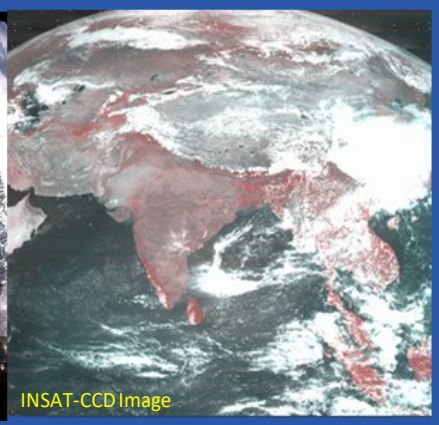
INSAT-CCD Image

Instrument: GISAT-1 is configured to provide imaging of Earth disk or region of interest from geostationary orbit (altitude 35786 km) with parking position at 93.5°E longitude The optical system consists of two-mirror modified RC telescope and field correcting optics. The orbit and instrument design of GISAT ensure high resolution frequent sampling of earth features. GISAT will carry an imaging payload capable of providing near-real time multi-spectral and hyper spectral images of a region. The multi spectral MX sensor has 6 bands and spatial resolution 42 m. The hyperspectral spectrometer has two modules HYSI-VNIR ((158 bands between 375-1000 nm and spatial resolution 320 m)) and HYSI-SWIR (256 bands between 900-2500 nm and spatial resolution 191 m). The hyper-spectral imaging in VNIR and SWIR bands are currently not available in Geostationary platform and would open up new areas of applications. The high spatial resolution multispectral MX instrument is capable of providing 'AWiFS' class imagery (available from Resourcesat-1/2/2A) during the entire sunlit period over India. Six bands of MX sensor include legacy four bands (Blue, Green, Red and NIR bands) available in earlier LISS-1/LISS-II/LISS-III/AWiFS sensors and two additional bands (Red edge and Split NIR). New channel such as red edge band 0.710 to 0.740 µm is useful for shape modelling and assessing vegetation biochemical properties and Split NIR band 0.845 to 0.875 µm is useful in reducing the effect of atmosphere by avoiding atmospheric water vapour absorption in NIR channel.

Scientific Requirements and Geophysical Products: The understanding of biodiversity, land use & land cover change, and the underlying processes is an important research area for assessment and management of resources needed for sustainable development. The earth observation from geostationary platform with suit of sensor systems operating in visible and infrared spectral region, with capability to spatially characterize natural ecosystems viz. forest, grasslands, wetlands, desert and coastal environments in varying scale and time provides a holistic view to each component of the ecosystem.

Phytoplankton forms the first link in the ocean food chain and gives an indication about the standing stock of green biomass, which helps in predicting the third level productivity. They also provide better understanding of the role played by ocean productivity in the uptake of carbon dioxide from atmosphere. Thus modeling primary productivity from space is important for tertiary resource assessment and maximum sustainable yield of

the resources. Marine living resources provide animal protein requirement of human being. An improved knowledge of identification of marine living resources is required to harness full potential of commercial fishery.

The land surface processes play an important role in regional/ large–scale climate modeling due to their role in providing the surface boundary conditions to energy/water exchange with the atmosphere. Land is a major component of climate system, but inclusion of land biophysical processes in climate models is still relatively simplistic. Remote sensing from satellites provides the only means of obtaining regular global land data to force and validate land surface processes in the climatic models. Land-atmosphere interactions have traditionally been described in terms of four sub-disciplines: bio-geophysical fluxes, biogeochemical fluxes, hydrology, and ecosystem dynamics. The land surface parameters such as surface albedos (direct beam and diffuse for visible and near-infrared wavebands), upward longwave radiation, sensible heat flux, latent heat flux, and surface wetness forms some of the important inputs in climate modeling.

The data products have been designed to meet the more general needs of regional monitoring, modeling, and assessment. The geophysical products have been categorized mainly in three categories, viz. Land surface Parameters, Ocean parameters and Atmospheric Parameters. The brief description of each type of parameters are as follows.

Land Surface

1.Atmospherically corrected Surface reflectance, 2.Vegetation indices (NDVI, EVI) , 3.Albedo, 4.Leaf area index (LAI) / fAPAR, 6.Gross primary productivity (GPP)

Ocean

1.Ocean suspended sediments , 2.Ocean chlorophyll, 3. CDOM+Detritus absorption, 4. Phytoplankton size class (PSC)

Atmosphere

1.Aerosol optical thickness, 2.Columnar water vapor content, 3.Cloud optical properties

Potential Applications: The high spatial resolution multispectral MX-VNIR instrument would provide data over entire country for natural resource assessment. The hyperspectral imaging in VNIR and SWIR bands at moderate spatial resolution is capable of providing advanced Ocean color Monitor capability. It will provide opportunity to retrieve ocean optics bio optical parameters for understanding the ocean biological processes. Operational retrieval of biophysical parameters like LAI, fAPAR, GPP, albedo and regional scale crop-nutrient-stress detection, fog detection and tracking dust storm etc. are some of the new applications. GISAT-1 data would help in carrying out following important applications.

Crop Monitoring at regional/national level, Drought progression and assessment, Flood Monitoring, Fog detection , Dust Monitoring, Cyclone track monitoring prediction, Now casting of weather systems, Input to Improved Weather Forecasting, Algal bloom Detection, Seasonal Wetland Monitoring, Seasonal Forest Growth assessment, Mapping and monitoring of snow cover,

The major user requirement for land/ocean related observations was imaging entire Indian landmass and surrounding areas during the sunshine period. Nominal imaging plan for GISAT-MX instrument is to acquire data for entire Indian landmass twice daily.

NISAR: Science and Applications

ANUP K DAS
Sci./Eng-SG, MTDD/AMHTDG/EPSA, Space Applications Centre (ISRO), Ahmedabad
anup@sac.isro.gov.in

NASA-ISRO dual-frequency Synthetic Aperture Radar (NISAR) is a collaborative mission jointly taken up by the Indian Space Research Organisation (ISRO) and the U.S. National Aeronautics and Space Administration (NASA) planned for launch in 2022. The NISAR mission has been conceptualized to provide L and S band space-borne SAR data with high repeat cycle, high resolution, and larger swath (>240 km) with capability of full-polarimetric and interferometric modes of operation. Towards the realization of NISAR payload ISRO is responsible for the development of S-Band SAR system while the Jet Propulsion Laboratory (JPL), NASA will develop the L-Band SAR system along with data recorder and GPS system. Both radar systems will share a common antenna reflector (12meters) provided by JPL/ NASA. NISAR will be launched by ISRO using GSLV-Mark-II launch vehicle.

NISAR is expected to provide an impetus to the fast maturing microwave remote sensing applications in geosciences. It is going to be the first mission to systematically and globally study the solid Earth, the ice masses, and the ecosystems. With larger swath achievable through SweepSAR technology combined with high spatial and temporal resolution, the dual frequency SAR will be highly suitable for land and ocean applications in regional to global scale. It is also expected to play a vital role in disaster response and monitoring for a country like India, which experiences recurring natural hazards such as floods, earthquakes, cyclones, landslides, avalanches and forest fires. Apart from that, the S-band SAR on-board NISAR would serve as a transition between C- and L-band, supporting new applications in vegetation and land surface mapping. The primary goals of NISAR are: 1) Characterize the global distribution and changes of vegetation aboveground biomass and ecosystem structure related to the global carbon cycle, climate and biodiversity; 2) Determine the likelihood of earthquakes, volcanic eruptions, and landslides through surface deformation monitoring; and 3) Predict the response of ice masses to climate change and impact on sea level. In addition, NISAR mission also has observa-

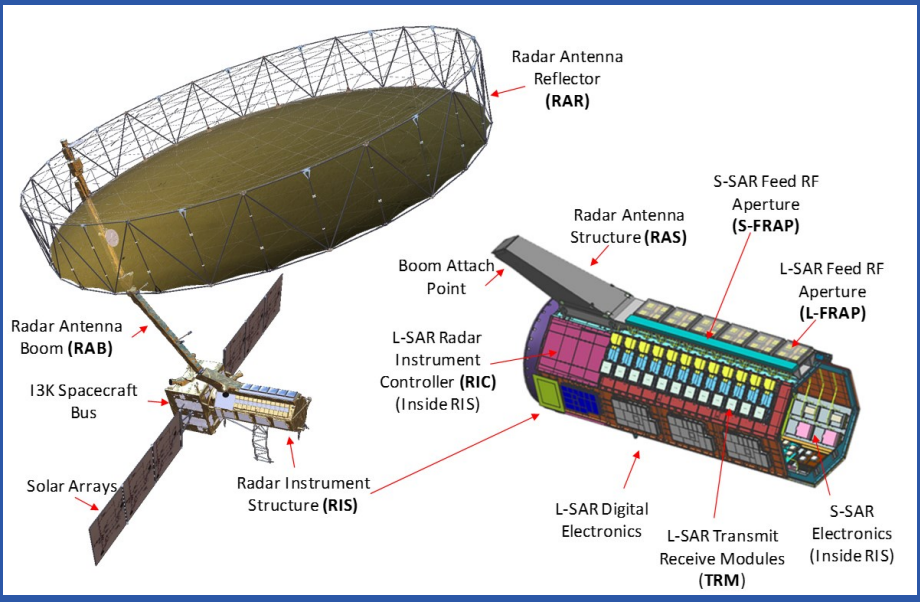

Figure 1: NISAR spacecraft in-orbit configuration and physical layout

tion plans to greatly improve monitoring of oceans, coastal regions, groundwater, hydrocarbon, and sequestered CO_2 reservoirs.

The nominal mission life of NISAR is 5 years. All NISAR science data (L- and S-band) will be freely available and open to the public. With its global acquisition strategy, cloud-penetrating capability, high spatial resolution, and 12-day repeat pattern, NISAR will provide a reliable, spatially dense time-series of radar data that will be a unique resource for exploring changes on Earth. Table-1 lists the instrument characteristics. Details of the NISAR mission and science plan are available in NISAR Science Users' Handbook (JPL-Caltech, 2018, p-320) available at: https://nisar.jpl.nasa.gov/files/nisar/NISAR_Science_Users_Handbook.pdf.

Table 1. Major mission and instrument characteristics of NISAR

Parameters	S-band	L-band
Orbit	747 km with 98° inclination	
Orbit / Pointing control	< 350m / < 273 arc seconds	
Repeat Cycle	12 days	
Time of Nodal Crossing	6 AM / 6 PM	
Frequency	3.2 GHz ± 37.5 MHz	1.257 GHz ± 40 MHz
Available Polarimetric Modes	Single Pol (SP): HH or VV Dual Pol (DP): HH/HV or VV/VH Compact Pol (CP): RH/RV Quasi-Quad Pol (QQP): HH/HV and VH/VV	SP: HH or VV DP: HH/HV or VV/VH CP: RH/RV Quad Pol (QP): HH/HV/VH/VV
Available Bandwidths	10 MHz, 25 MHz, 37.5 MHz, 75 MHz	5 MHz, 20 MHz, 40 MHz, 80 MHz (Additional 5 MHz iono band for 20 & 40 MHz modes at other end of pass-band)
Swath Width	> 240 Km (except for QQP Mode)	> 240 Km (except for 80MHz BW)
Spatial Resolution	7m (Az); 3m-24m (Slant-Ra)	7m (Az); 3m-48m (Slant-Ra)
Incidence Angle	33 – 47 deg	
Noise Equivalent Sigma0	-25 dB (baseline) -20 dB (Threshold)	-25 dB (for required full-swath modes)
Ambiguities	< -20dB for all modes except QQP	< -23dB swath average in SP or DP modes < - 17dB swath average in QP mode
Data and Product Access	Free & Open	

NISAR has been planned as a science mission, however, ISRO finds a lot of potential in NISAR data for applications related to ecosystems, cryosphere, coasts, oceans and deformation studies. The science team of NISAR has recommended enhanced coverage of south polar region as several other contemporary SAR missions have observation plans inclined towards coverage of north polar targets. Accordingly, NISAR would be operated primarily in left-only looking mode to cover Antarctica up to 87.5°S latitude. There is also a plan to roll-tilt the satellite to image entire Antarctica as a campaign mode once during the mission. Fixing the left-only looking mode for NISAR would result into a larger polar hole in the Arctic region (beyond 77.5°N latitude) during nominal mission. The primary science objectives of NISAR mission are categorized into the following themes:

Ecosystem structure: Major objectives under this theme include monitoring changes in ecosystem structure and biomass in Indian region; agriculture biomass and crop monitoring; soil moisture estimation over bare and crop covered soils, forest biomass estimation, biomass change and carbon sequestration monitoring; mangroves and wetlands characterization; alpine forest characterization and delineation of tree-line ecotone.

Land deformation: Major objectives under this theme include measurement of deformation due to co-seismic and inter-seismic activities; landslides; urban land subsidence and volcanic deformation.

Cryosphere studies: Major objectives under this theme include measurements of dynamics of polar ice sheet – ice shelf – glacier; sea-ice types, thickness and motion; land ice velocity and ice discharge to the ocean; Himalayan snow and glacier dynamics

Oceanography: Major objectives under this theme include retrieval of ocean physical parameters such as surface wind speed, wave spectra; coastal bathymetry; identification of upwelling zones; and ship detection

Coastal processes monitoring: Major objectives under this theme include understanding of the coastal erosion processes through the study of near -shore dynamics and coastal subsidence; assessment of coastal vulnerability to sea-level rise and shore-line change and coastal habitat.

Geological studies: Major objectives under this theme include mapping of structural and lithological features; lineaments and paleo-channels; geomorphological mapping; mineral explorations and geo-archaeology.

Disaster response: Major objectives under this theme include mapping and monitoring of floods, forest fires, oil spills, earthquake damage and mapping damage extents of extreme weather events such as tropical cyclones.

NISAR would observe entire global landmass including the cryosphere, polar oceans and Indian coastal oceans. The requirement of imaging parameters such as frequency, polarization, spatial resolution, backscatter ambiguities and temporal coverage are different for different applications. In order to meet the data requirements for various applications, several operation modes have been defined for NISAR. Table-2 describes the observation strategy of NISAR and Fig. 3 presents Indian and global targets identified for NISAR.

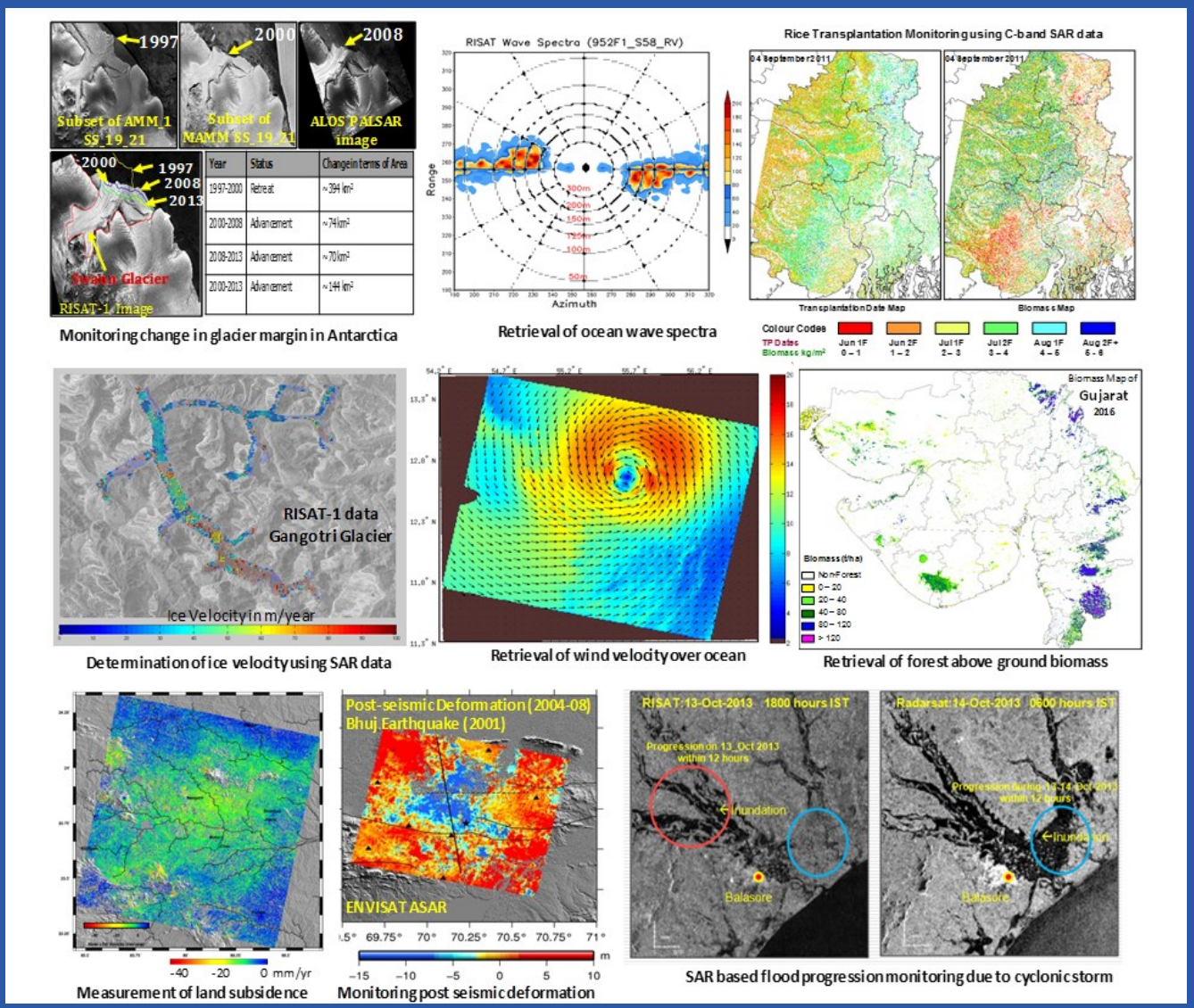

Figure 2: Examples of SAR applications in geosciences and disaster management

Table 2. NISAR observation strategy over global targets

Observation Strategy	L-band		S-band		Sampling Scheme	
Science Targets (colours as presented in the maps below)	**Mode**	**Resolution (Az × Ra)**	**Mode**	**Resolution (Az × Ra)**	**Desc. (D) Asc. (A)**	**Culling Approach**
Background Land (Global)	HH/HV	7m × 12m	-	-	A + D	Culled above
Land Ice	HH	7m × 3m	-	-	A + D	Culled above
Sea Ice Dynamics	VV	7m × 50m	-	-	A + D	-
Urban Areas - Global	HH/HV	7m × 6m	-	-	A + D	-
US Agriculture	QP	7m × 6m	-	-	A + D	-
Background Land (India)	HH/HV	7m × 6m	CP	7m × 6m	A	-
Himalayan Cryosphere	QP	7m × 6m	CP	7m × 6m	D	-
Indian Agriculture/ Forest/ Wetland	QP	7m × 6m	CP	7m × 6m	D	-
Indian Coastal Ocean	VV/VH	7m × 12m	CP	7m × 12m	A + D	-
Indian Seas (BoB and Arb Sea)	VV	7m × 50m	VV/VH	7m × 80m	A	-
Indian Urban Area/ Landslide zones	HH/HV	7m × 6m	HH	7m × 2m	D	-
Priority Ice (India)	VV/VH	7m × 12m	CP	7m × 12m	A + D	Culled
Land Deformation - Indian Region	HH/HV	7m × 6m	HH/HV	7m × 12m	A	-
Antarctica & Greenland Mosaic	-	-	CP	7m × 12m	A + D	Culled

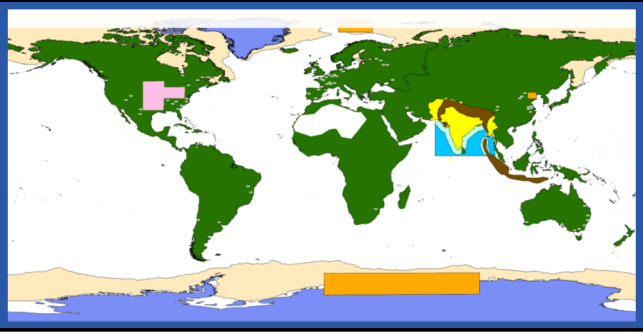

Ascending orbits

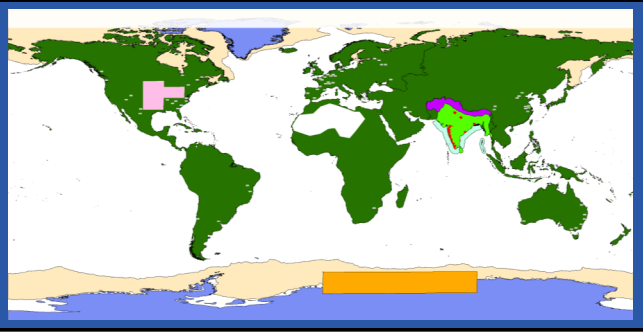

Descending orbits

Figure 3: Maps showing NISAR observation plan over Indian and global targets through Ascending and Descending orbits

HARNESSING ENERGY FROM OCEANS

SURISETTY V V ARUN KUMAR, RASHMI SHARMA AND RAJ KUMAR

EPSA, Space Applications Centre (ISRO), Ahmedabad

arunkumar@sac.isro.gov.in

INTRODUCTION

Recent studies have revealed that anthropogenic greenhouse gases cause havoc to the Earth's climatic system including oceans, land, and ecosystems (IPCC, 2007). With the exhaustion of fossil fuels and increasing awareness on these environmental issues, harnessing energy from renewable resources has become prime focus in the developing countries (Yan et al. 2010). Due to increased pressure of population and urbanization, many nations have understood that the ever growing demand for electrical energy can only be sufficed with the exploitation of new and renewable energy resources. India has the fifth largest power generation capacity in the world and its current renewable energy contribution stands at 17.3% of the total installed capacity (Figure 1) as on 2017. The Government of India has setup an ambitious target of renewable energy capacity to 175 GW by end of 2022, committed to Clean and Green Energy and is driving efforts to achieve 40% power installed capacity from non-conventional energy resources and reducing emissions by 33- 35% of its GDP by 2030. This target includes 100 GW of solar power (including 40 GW of grid-connected roof-top solar installations), 60 GW from wind power (including onshore and offshore wind farms), 10 GW from biomass power and 5 GW from small hydro power. India stands fourth largest installed capacity of wind power mostly from onshore wind farms. The presence of strong and persistent winds all throughout year, many regions along the coast of India are suitable for good potential of wind energy.

However, assessing such resources requires accurate long-term measurements. However, in a developing country like India, offshore meteorological buoys is sparse and such observations are highly expensive. Hence, satellite remote sensing could provide synoptic data, covering larger areas continuously for longer periods. Wind and waves can be monitored using space-borne microwave radars like scatterometers and altimeters respectively in the polar orbits. Wave-power generation is not currently a widely used technology. With the advent of latest satellite technology, many scatterometers and altimeters are available e.g., OSCAT, the Ocean Scatterometer on-board OCEANSAT-2 from India Space Research Organisation (ISRO), SeaWinds on-board QuikSCAT from the National Aeronautics and Space Administration (NASA), advanced scatterometer ASCAT on-board Metop-A and Metop-B of the European Organisation for the Exploitation of Meteorological Satellites (Eumetsat), SARAL-AltiKa (Ka band radar altimeter), Jason-2, 3 (Ku-band altimeters) etc catering the needs of different applications for the scientific community. In this paper, both Ku and Ka-band of altimeters are used for identification of the potential regions of wave power. Since scatterometer derived winds are not available over the land, analyses from Numerical Weather Prediction Models (NWP) like Weather Research and Forecasting Model (WRF) derived winds are generally used to estimate wind energy and the same model was used to forecast solar energy also.

At Space Applications Centre (SAC), a large volume of satellite datasets on winds, insolation and waves have been utilised from several Indian and foreign satellite datasets synergistically to generate a valuable information on the availability of renewable resources in India. The present work discusses on various methods used to generate such datasets and the major applications on solar, wind and wave energy. We also carried out some experiments and issued forecasts of solar and winds using WRF model including satellite data assimilation. The forecast can be accessed through VEDAS (https://www.vedas.sac.gov.in).

Wind Energy

Scatterometers are the missions with specific goal of observing the equivalent-neutral surface ocean vector winds across the world. Orbit-wise scatterometer wind products at 12.5 km spatial resolution from QuikSCAT (L2B version 3), OSCAT (L2B version 2) for the whole mission period 2000-2009 and 2010-2014 respectively and ASCAT (L2B version 2 coastal winds) for 2012-2016 have been processed to generate long-term synoptic monthly means in the Indian region (Lat.0-25^{o}N; Long. 65-95^{o}E). The mission targeted wind vector precision and accuracy are, respectively, 3.0 m s^{-1} for ASCAT, 0.5 m s^{-1} for QuikSCAT and OSCAT. The wind energy density, E is calculated from the Weibull parameters using the gamma function G and the air density r (~1.225 g m^{-3}) at sea level as

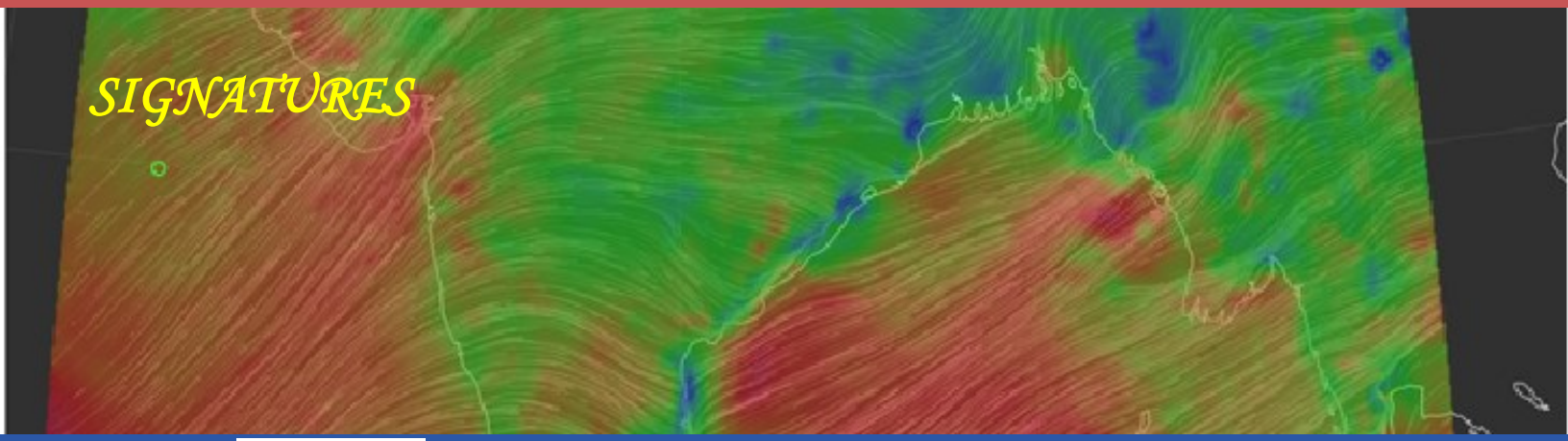

$$E = \frac{1}{2}\rho A^3 \Gamma\left(1+\frac{3}{k}\right) \quad (1)$$

Where A and k are the Weibull scale and shape parameters.

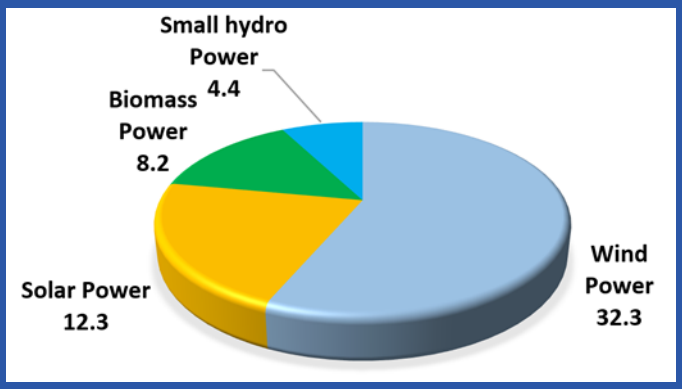

Figure 1: Renewable energy installed capacity (GW) in India as on June 2017 (source: MNRE)

The retrieved wind speed is 10 m height above the sea surface, while the height of wind turbine hub is mostly 60 – 100 m above the sea surface. In this consequence, the wind energy density should be calculated before wind power evaluation. Wind speed at hub height h is obtained by means of logarithmic law

$$v_h = v_o\left(\frac{\log\left(h/z_o\right)}{\log\left(10/z_o\right)}\right) \quad (2)$$

Where v_o is the wind speed at height 10 m above the sea level and z_o is the roughness length typically equal to 0.0002 m at the sea surface. Using Weibull probability density function, the shape parameter k_h and scale parameter c_h at desired height *h* were calculated using Safari and Gasore, (2010) and thus the energy density at hub height was calculated by Equation (1). The power generated by a turbine was computed following Mathew (2006)

$$P_{turbine} = \int_{v_i}^{v_o} P(v) f(v)\, dv \quad (3)$$

Where *P(v)* is the power expected for a wind velocity (*v*) derived from power curve of a turbine, *f(v)* is the probability density function of Weibull distribution derived from A and k parameters. The practical power production expected from a wind turbine was computed using the power curve of a RE-power Systems 5M (REpower 5M) turbine in the offshore waters. The minimum "cut-in" (v_i), rated (v_r) and maximum "cut-off" (v_o) velocities of this turbine are 3.5, 13 and 30 m/s, respectively.

Wave Energy

Wave Energy from Altimetry

Altimeters do not provide any direct measurements of the wave power. Employing the significant wave height (SWH) and wind speed measurements, the wave period is calculated. This computation is based on the data adaptive techniques of genetic algorithm following Remya et al (2011). The SWH and wave period is then used for computation of wave power. Thus in order to compute the wave power, the wave period estimated from altimeters is validated using the in-situ observations from the INCOIS buoys. The satellite observations used include the Altimeter measurements of Jason-2 from 2008-2014 and SARAL/AltiKa from 2013-2014. The equation for deriving wave power is given by

$$P_{wave} = \frac{\rho g^2}{64\pi} H_{m0}^2 T \approx \left(0.5\frac{kW}{m^3.s}\right) H_{m0}^2 T \quad (4)$$

Where, P_{wave} is Wave power per unit of wave–crest length, H_{m0} is the significant wave height, ρ is the density of water, g is the acceleration by gravity and *T* is wave period. According to this formula wave power is proportional to wave period and square of wave height.

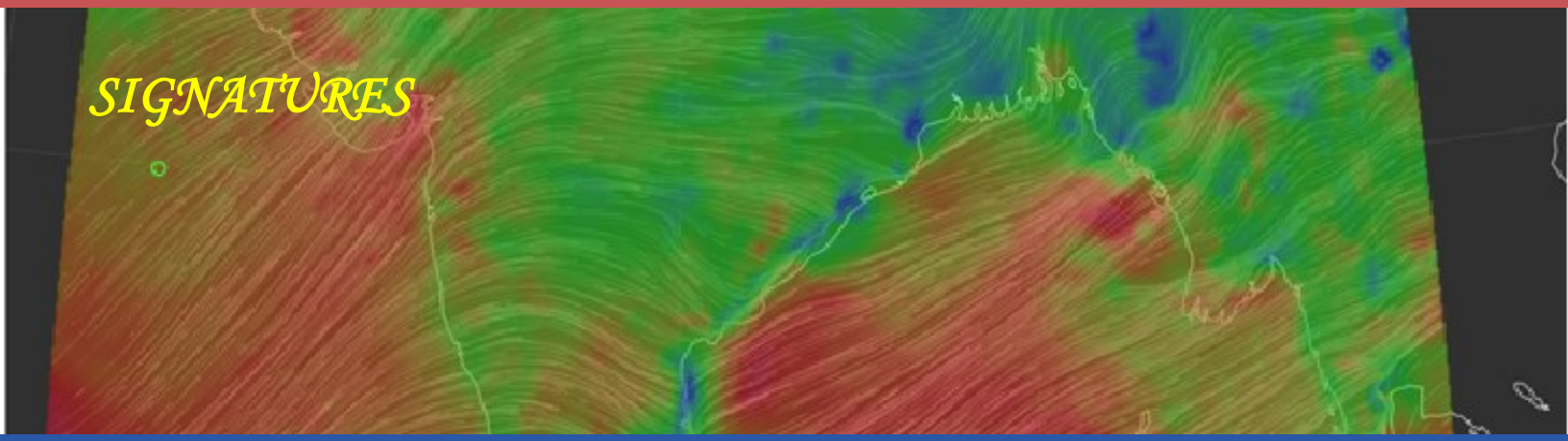

Wave Energy from Numerical model

We have also used the Wave Watch-III model at 10 km resolution to assess the wave energy near the Indian coast. The model was run with ECMWF wind data and a monthly climatology has been constructed using this data to introspect the numerical model based wave energy assessment.

The synergetic monthly maps of wind energy combining QuikSCAT, OSCAT and ASCAT are shown in Figure 7. The combination is done by collecting samples from each satellite using a regular grid of 0.125°. Later, the scale and shape parameters for Weibull fitting have been estimated and energy density has been computed using the equation (1). The winds show a strong seasonal variability owing to Indian Summer Monsoon (ISM). The mean wind speeds derived from scatterometer data for the whole period are around 7 – 12 m s^{-1} along Kanya Kumari and Saurashtra coast (Surisetty et al. 2016). Although the wind energies are higher in the deep ocean, it is practically not feasible to extract wind power at such greater depths (>1000 m). West coast of India having wider continental shelf with more length along the Gujarat coast, makes practically viable for offshore wind farming. Although southern Tamilnadu coast is having higher wind energy potential, the depths are higher due to narrow continental shelf. Based on these monthly maps, we found that the wind energy/power is significantly higher at the Rameswaram-Kanyakumari (>1500 W m^{-2}) region throughout the year thus indicating the potential of this regions for setting up of offshore wind energy farms. The annual electric power production possible from a REpower 5MW turbine that could be extracted is around 3500 KW around Rameswaram coast and near Saurashtra region, it is around 2500 KW (Figure 2).

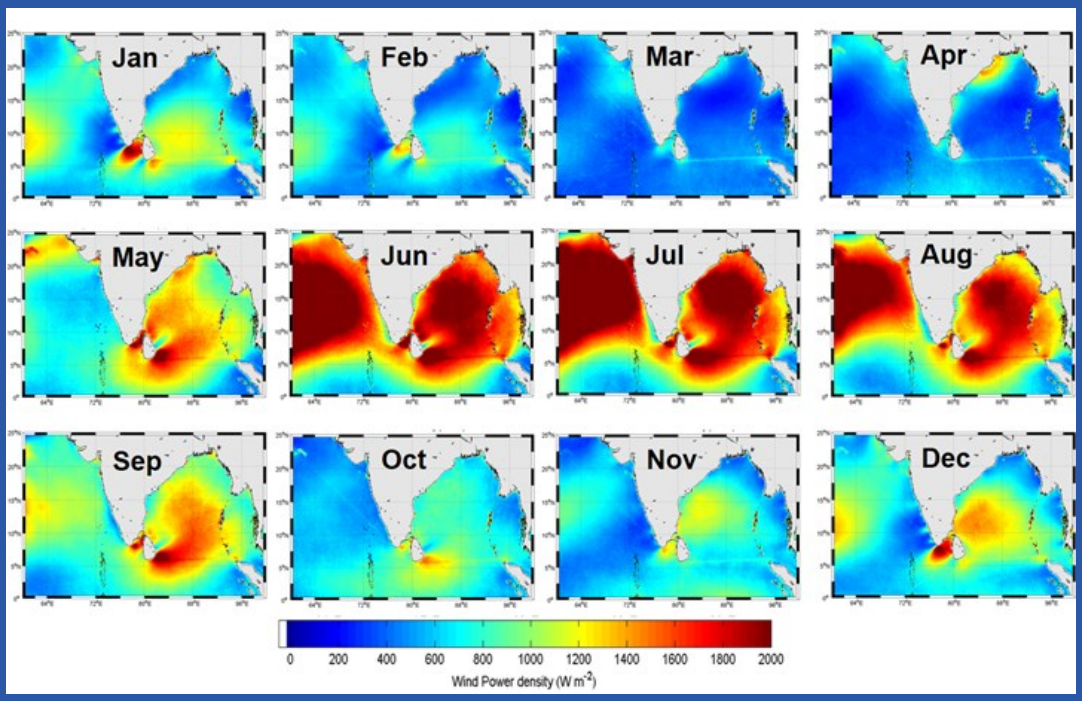

Figure 2: Monthly wind power density at 80 m height derived from QuikSCAT (2000-2009), OSCAT (2010-2014) and ASCAT (2012-2016) scatterometer data extrapolated using logarithmic law.

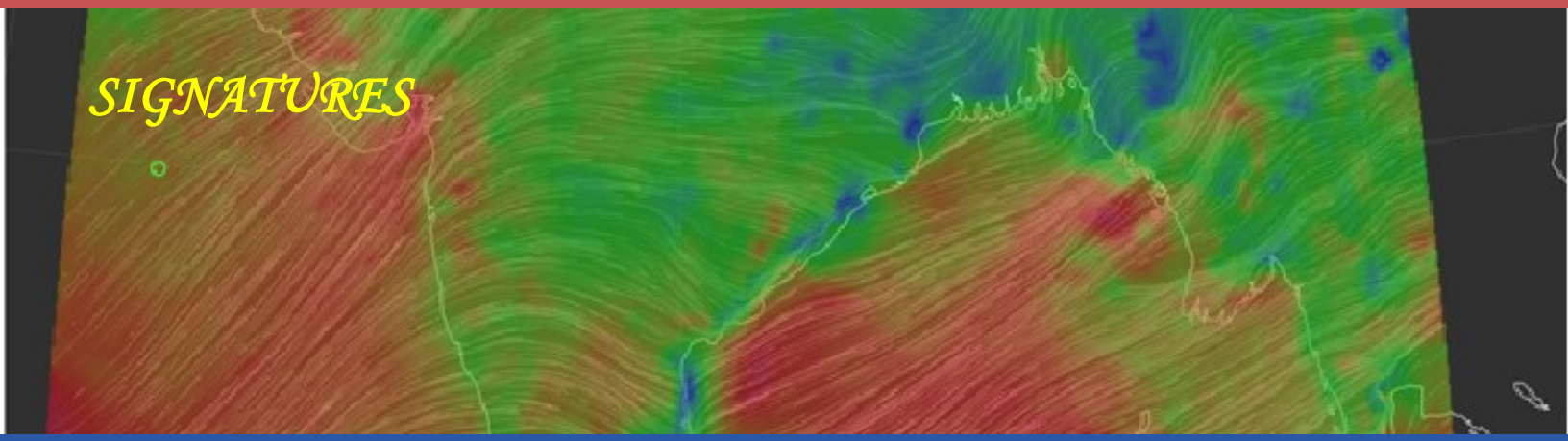

Wave Energy

In addition to the solar and wind energy, India has very good potential of wave energy, but it is less explored and not currently a widely employed commercial technology. Wave power is generally extracted using wave energy converter (WEC), which can be deployed like a mooring system on the surface of water and then the electrical energy can be transferred to the land by electrical lines. Using different satellite altimeters, we had attempted to assess the total wave power in the Indian waters. The average wave power was computed for each month of 2008-2014 in order to analyse the inter-annual variability of the wave based power over the Indian Ocean region. Figure 3 shows the monthly derived wave power potential in the Indian waters.

Dissemination of Renewable energy data through VEDAS portal

VEDAS portal (http://vedas.sac.gov.in) provides access to various applications on different themes developed at SAC (Figure 4). The details of different renewable energies like solar, wind and wave can be accessed through web portal or through any smart phone. .

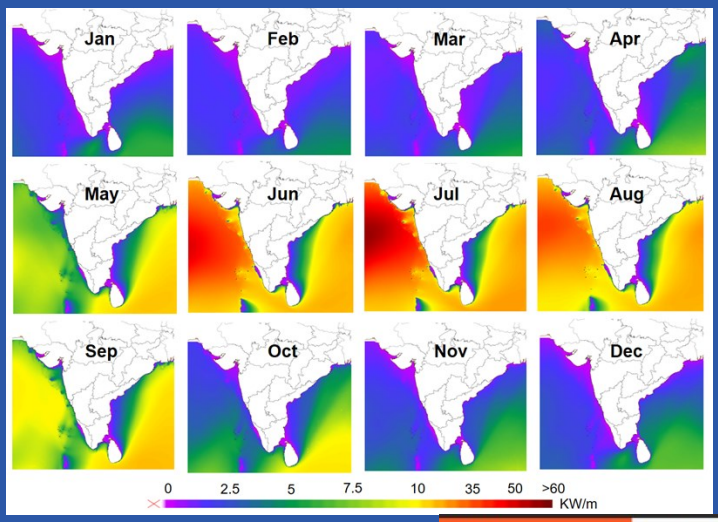

Figure 3: Monthly Wave power climatology derived from Wave Watch –III model assimilated by satellite data

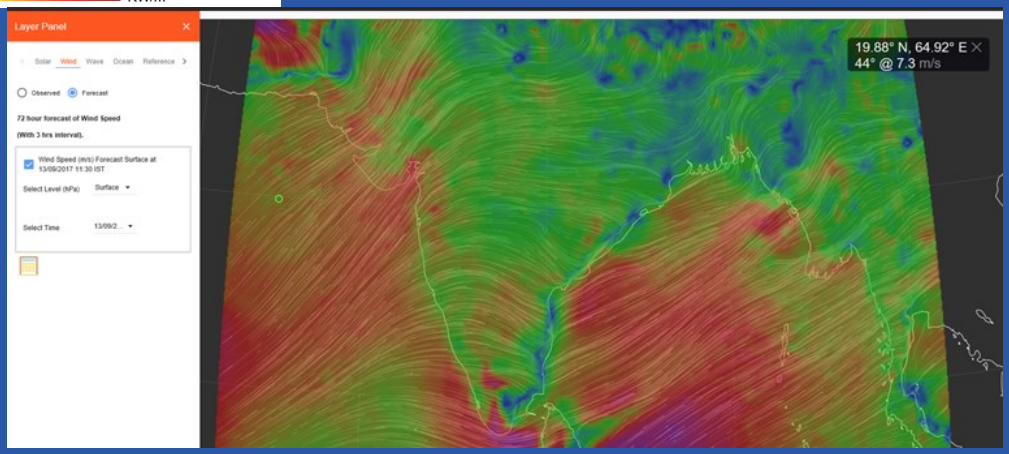

Figure 4: Web view of wind forecast dissemination through VEDAS

Assessment of coastal erosion along the Indian coast

RATHEESH RAMAKRISHNAN, PREETI RAJPUT and A S RAJAWAT
GSD/GHCAG/EPSA, Space Applications Centre (ISRO), Ahmedabad
ratheeshr@sac.isro.gov.in

The long stretch of coastline on either side of the Indian peninsula is subjected to varied coastal processes and anthropogenic pressures, which makes the coast vulnerable to erosion. Planning measures for sustainable development along the coastal region require a systematic inventory of shoreline changes occurring along the entire Indian coast on 1: 25,000 scale. It is in this context, the Coastal Protection and Development Advisory Committee suggested to generate database of shoreline changes mapped on 1: 25,000 scale for the entire Indian coast based on multidate remote sensing data in GIS environment. Shoreline change database has been prepared based on the satellite data for 1989–1991 and 2004–2006 time frame and shoreline change atlases were prepared. The results show that 3829 km (45.5%) of the coast is under erosion, 3004 km (35.7%) is getting accreted, while 1581 km (18.8%) of the coast is more or less stable in nature. Highest percentage of shoreline under erosion is in the Nicobar Islands (88.7), while the percentage of accreting coastline is highest for Tamil Nadu (62.3) and Goa has the highest percentage of stable shoreline (52.4). The analysis shows that the Indian coast has lost a net area of about 73 sq. km during 1989–1991 and 2004–2006 time frame. Recent LISS-4 satellite data of 2014-16 time frame is used to update the shoreline and the shoreline change database is prepared in GIS format. The results shall form the baseline data for various concerned central and state government agencies to identifying eroding coastal stretches and to carry out coastal protection measures.

Introduction

Issues related to coastal erosion can be viewed in two different aspects; one where the erosion rates are low but the threat of coastal erosion is for a longer timescale and while

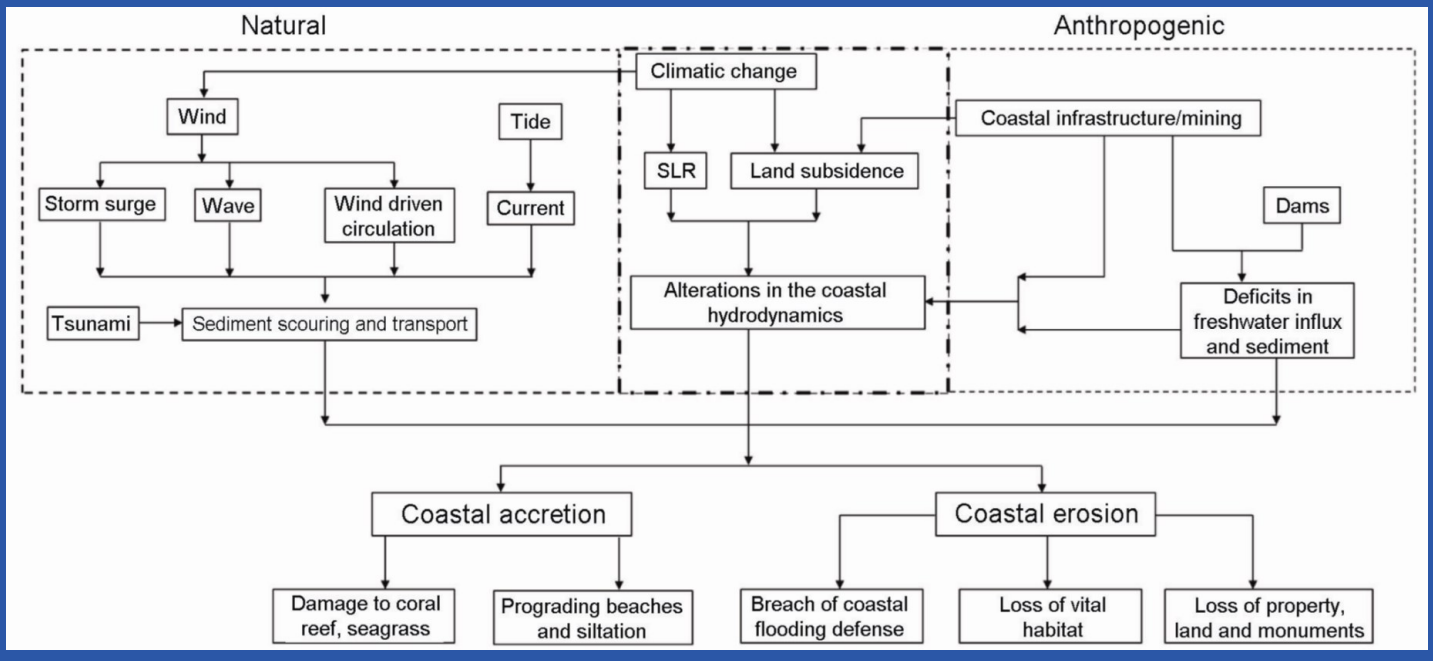

Figure 1. Schematic diagram representing the coastal erosion processes

the second one is an ephemeral process, mostly concurrent with sporadic events and usually the loss permanent loss of land, even though a slow process, poses a significant threat to valuable land, property and natural coastal resources, including vital habitats. Anthropogenic pressures along the region have significant contribution towards the incessant coastal erosion. Inevitable development activities along the coast and in the catchment areas of the river have induced changes in the equilibrium of the sediment transport which cause undesirable accretion and erosion along the coast. The rise in sea level and local coastal subsidence also lead to changes in the coastal processes (Nicholls and Cazenave, 2010). Coastal erosion during storm surge, tsunami or even monsoonal high wave period usually evolves into disaster, but the impact on coastal erosion will be for a shorter period (Erosion, 2004). Figure 1 shows a schematic diagram involving coastal erosion processes.

Coastal erosion, as in other maritime countries, is a serious problem along the Indian coast. India, as it forms a peninsula, has a long coast on its east and west regions with varied coastal processes dominating the coastal dynamics. These include tide-dominated regions along the northern parts of the west coast, open coast with high wave energy along the southern parts of the west coast, strong longshore sediment transport along the southern parts of the east coast and the coast strongly influenced with river discharges along the northern parts of the east coast. The coastal geomorphology and the land-use pattern along the Indian coast also show a varied range, which includes coral reefs, mangrove belts, tidal mudflats, rocky coasts, wide sandy beaches and deltaic and bay environments.

The Indian coast is relentlessly modified by the mounting development activities along the coastal region, which under improper management at times leads to severe coastal erosion. Management plans with proper understanding of the coastal processes and coastal dynamics are needed to achieve sustainable development along the coastal region, where planning measures have to be taken up at the national level. Inventory related to coastal erosion are a prerequisite in understanding the coastal dynamics of the region. Even though there are studies and inventory of coastal erosion and littoral sediment transport along the Indian coast, they are region-specific (Bhatti et al, 2018; Muthusankar et al, 2017; Sowmya et al, 2019; Ratheesh et al, 2017) and inadequate for planning-level requirements at the national level.

Shoreline detection using satellite images

Coastal land-use/land-cover maps have been prepared for the entire Indian coast on 1 : 25,000 scale using Resourcesat-2 LISS-IV data for 2014_16 period, IRSP6 LISS-IV data of 2004 –2006 period and SPOT-1 and 2 multispectral and IRS-1A and IRS-1B LISS-II data of 1989–1991. Geospatial database is created for 2004_06 and 1989_91 period that forms a part of Coastal Zone Information System (CZIS) developed at Space Applications Centre (SAC), Ahmedabad. These maps also depict High Tide Line (HTL) and Low Tide Line (LTL). Shoreline change mapping for the purpose of demarcating coastal erosion, accretion and stable nature of the coast has considered changes in HTL as these exclude seasonal changes, where HTL represents Highest High Tide Line.

On screen digitization of the HTL has been carried out based on the geomorphic indicators (NCSCM, 2015). Image interpretation keys based on Nayak et al (1991) is used to identify the geomorphic indicators to delineate the HTL that are based on various geomorphologic/ land-use features and tonal contrasts like landward berm/dune crest, rocks, headlands, cliffs, seawalls or embankment, permanent vegetation

line, landward side of mangroves, salt pans, supra-tidal mud flats, etc.

The HTL is prepared for all maritime states and Union territories of India on 1:25,000 scale. One degree consists of 8X8 rectangular grids or cells. Each rectangular grid or cell represents one SOI topographic area on 1:25,000 scale. Spatial layer of Point of habitation and line layer of rail and road are taken from CZIS database. Spatial analysis techniques are used to compute the spatial shift among the HTL of different time frame. Polygons for areas under erosion and accretion were created. Areas under erosion and accretion were measured for the main shoreline (excluding creeks, river mouths, estuaries). Shore length under erosion, accretion and stable categories were measured for the main shoreline (excluding creeks, river mouths, estuaries). Figure 2 shows examples of geomorphic features identified as HTL from satellite images and corresponding field photos.

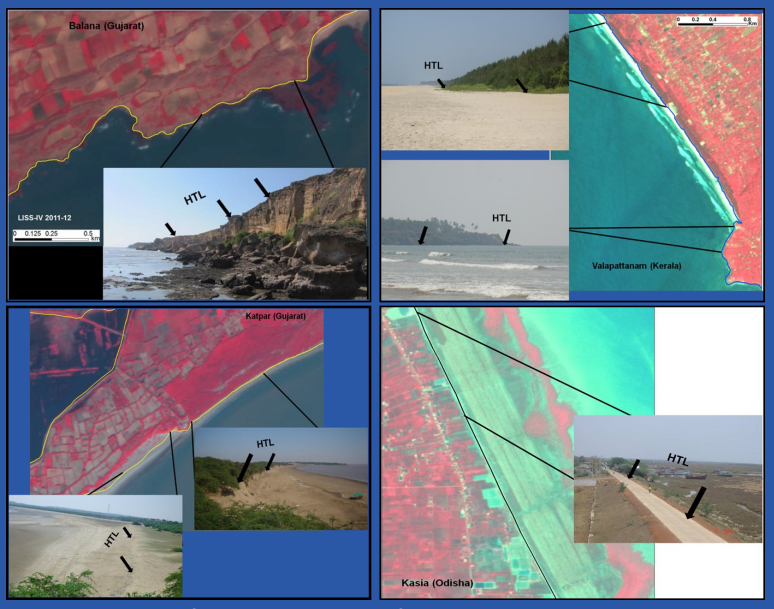

Figure 2: Different geomorphic features used to delineate

Shoreline change statistics

According to the shoreline change inventory between 1981-91 to 2004-06 period, the total length of the main shoreline, which excludes the length of the mouth of estuaries, rivers, creeks and the inner part is 8414 km (Rajawat et al, 2015). Andaman Islands has the longest coastal length ~1722 km and Lakshadweep Islands has the smallest coastal length of about ~136 km. Out of the 8414 km length of the Indian shoreline, around 45.5% (3829 km) is observed to be under erosion (Figure 2). Accretion has occurred along 35.7% (3004 km) of the shoreline while 18.8% (1581 km) of it is observed to be more or less stable. The Maritime state-wise distribution of shoreline length under erosion, accretion and as stable is shown in Figure 3. The length of shoreline under erosion is longest for Andaman Islands (740.34 km) and it is shortest for Goa (27.03 km), while the shoreline length that has accreted is also maximum for Andaman Islands (944.84 km) and minimum for West Bengal (19.46 km).

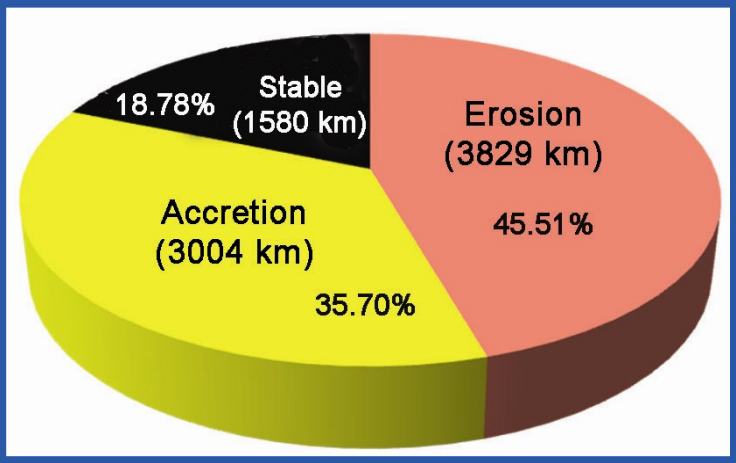

Figure 3 :Length of shoreline under erosion, accretion and as stable along the entire Indian coast.

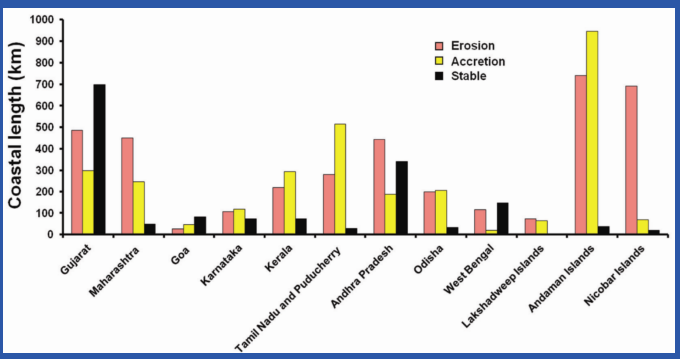

Figure 4: Coastal length under erosion, accretion and as stable in different Maritime states/UTs (excluding mouths of rivers/streams/creeks and their inner parts).

While assessing the percentage-wise distribution of shoreline length under erosion, accretion and as stable for individual Maritime states and UTs, Nicobar Islands show the highest percentage of shoreline under erosion (88.7), followed by Maharashtra and Lakshadweep (Figure 5 a). For the remaining Maritime states, the eroding shoreline length is less than 50% of their total respective shoreline lengths. Percentage of accreting coastline is highest for Tamil Nadu, which is around 62.3% of its total shoreline (Figure 5 b), followed by Andaman Islands, while least accretion is observed for West Bengal coast. Goa has the highest percentage of stable shoreline, which is about 52.4% of its total shoreline (Figure 5 c), followed by West Bengal, Gujarat, Andhra Pradesh and Karnataka coasts having around 20–40% as stable coast with respect to their total coastal length. The coast along Kerala, Odisha, Maharashtra, Tamil Nadu, Puducherry, Nicobar Islands, Andaman Islands and Lakshadweep Islands shows less than 10% as stable in general.

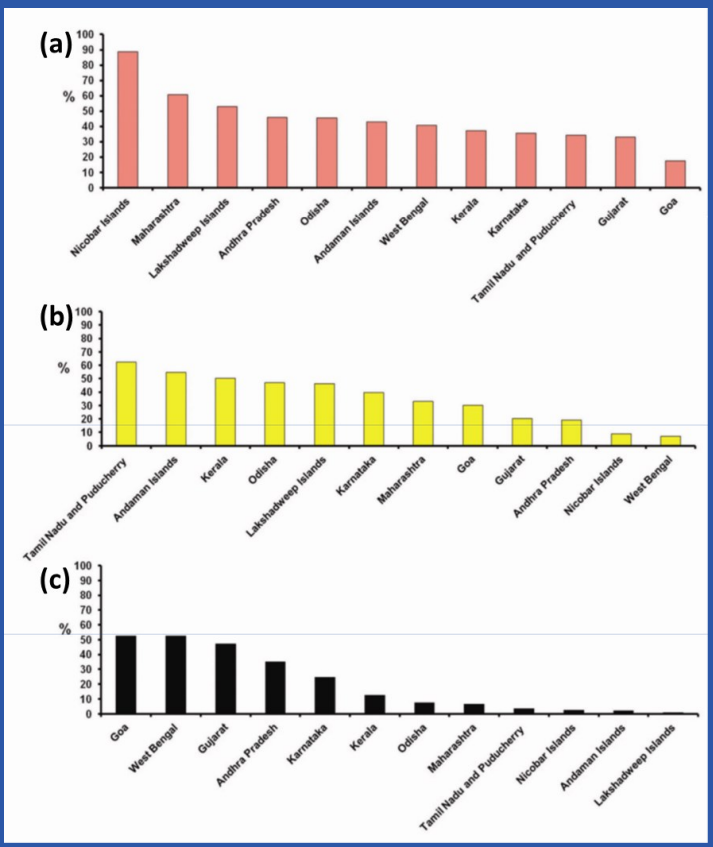

Figure 5: Percentage wise distribution of coastal length under erosion (a), accretion (b) and stable (c) in different Maritime states/UTs

Among various Maritime states and UTs, Tamil Nadu has the highest net increase of its coastal area which is about 25.45 sq. km, while net loss of coastal area is maximum for the Nicobar Islands, which is around 94 sq. km. Maharashtra, Andhra Pradesh, Odisha, West Bengal, Lakshadweep Islands and Nicobar Islands have a net loss of area, while the other Maritime states and UTs have a net gain along their coastal regions. The analysis also shows that the Indian coast has lost a net area of about 73 sq. km during 1989–1991 and 2004–2006 time frames.

Figure 6 shows selected hotspots along the Indian coast overlaid with the HTL of 2004–2006 and 21014-16 along with erosion and accreting regions. The figure elucidates the different aspects of coastal issues along the Indian coast. The major natural processes involved in the shoreline dynamics are a) migration of spit b) reduction of sediments from the river c) construction of coastal structures d) beach mining e) shoreline orientation.

The inventory along with current status of coastal protection measures taken up by concerned state departments has been used to prepare a Shoreline Change Atlas of the Indian Coast. The baseline data are aimed towards initiating appropriate action for protecting the Indian coast by concerned Maritime states and UTs besides use by the scientific community as well decision makers of the country.

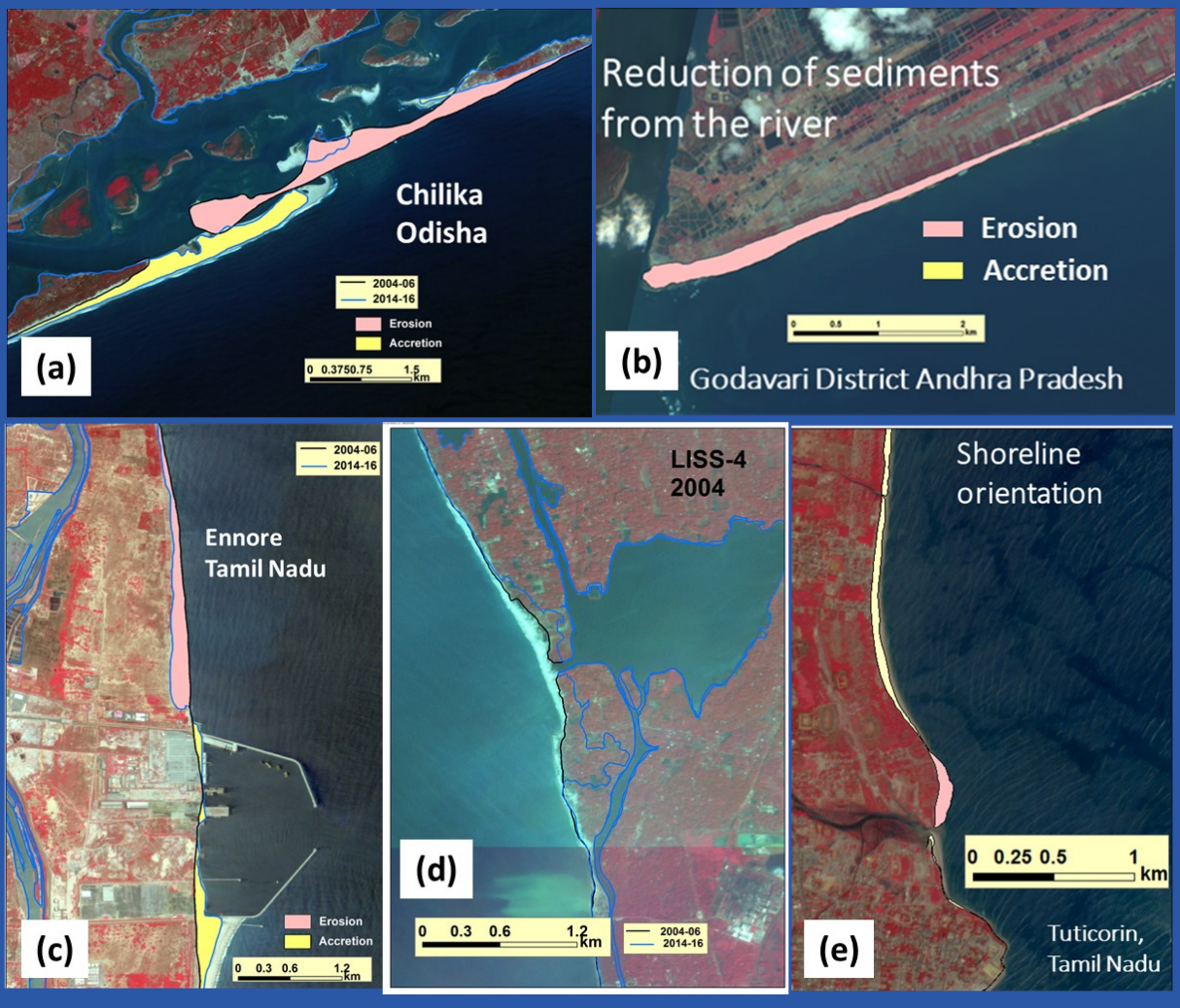

Figure 6: Hot spot regions of shoreline changes and various processes leading to the dynamics of the coastal region

Geophysical Applications of Satellite Altimetry

K M SREEJITH AND A S RAJAWAT
GSD/GHCAG/EPSA, Space Applications Centre (ISRO), Ahmedabad
sreejith@sac.isro.gov.in

Introduction

Altimeter derived geoid undulation and free-air gravity anomalies over world oceans are important data to understand lithospheric structure and plate tectonic processes such as sea-floor spreading, subduction of plates, continental margin evolution, under sea volcanism and fracture zone formation etc. In addition, high resolution marine gravity data provide an important resource for off-shore exploration. The main objective of this article is to introduce marine geophysical applications of satellite altimetry with few demonstrative case studies.

Estimation of Marine Gravity from Satellite Altimetry

The calculation of marine gravity field of the Earth from radar altimetry data is based on the principle that the sea surface corresponds to an equipotential surface of the gravity field. The presence of lateral density variations (e.g. seabed morphology and varying density of subsurface masses) distorts the shape of the gravity field and, by implication, the shape of the equipotential surface. The sea surface (or geoid) will bulge upwards over excess mass (gravity high) and will dip downwards over a mass deficit (gravity low). The Sea surface height (SSH) measurements from satellite altimeters averaged over a period of time represent the marine geoid. However, SSH need to be corrected for dynamic components introduced by currents, tides and other oceanographic and atmospheric phenomena. The deflection of geoid from the reference ellipsoid or geoid undulation could be calculated as the height of the satellite above the reference ellipsoid is precisely known (Figure 1).

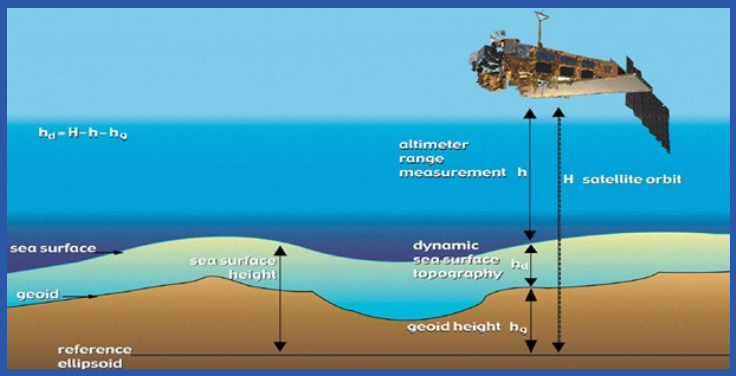

Figure 1: Measurement of Sea Surface Height from radar altimeter.

2.1 Altimeter missions for geodetic applications

Altimeters are generally operated at exact repeat cycles to provide high temporal sampling for for recovering changes in ocean surface height associated with currents and tides. However, marine geodetic applications require spatially dense satellite tracks. This is achieved by keeping satellite altimeters in "geodetic orbit" ie. an orbit with very long repeat cycles. The sources of geodetic altimeter data are the Geosat-GM (18 months), ERS-1 (11 months), Jason-1 (16 months), CryoSat-2 (since 2010), Jason-2 LRO (Since mid-2017-till date). It is noteworthy that since mid-2016 the SARAL/AltiKa satellite is operating in "Drifting Phase (DP)", similar to the geodetic orbit. SARAL/ALtiKa, being a Ka band sensor has better precision in measuring Sea surface height (~2 times than ENVISAT) and is extremely important to improve the short wavelength gravity field. SARAL/AltiKa data is proven to be efficient in detecting unchartered seamounts with better precision compared Ku band altimeters (Marks and Smith, 2018).

2.2 Regional gravity field of Indian Ocean

Space Applications Centre produced residual/prospecting geoid and gravity anomaly data over the Indian offshore using Geosat and ERS-1 data sets (Majumdar et al., 1998). Later, these data sets where up-dated using high resolution gravity data of Hwang et al., (2002) and produced value-added products in the form of different wavelengths residual/prospecting geoid and gravity anomaly maps (Majumdar and Bhattacharya, 2004). Further, Sreejith et al., 2013 implemented advanced techniques for retrieval of geoid and gravity from satellite altimeter and generated revised geoid and gravity data over the Indian offshore (Figure 2). An updated geoid/gravity data for the Indian Ocean region is being generated using a combination of SARAL/AltiKa and JASON data sets.

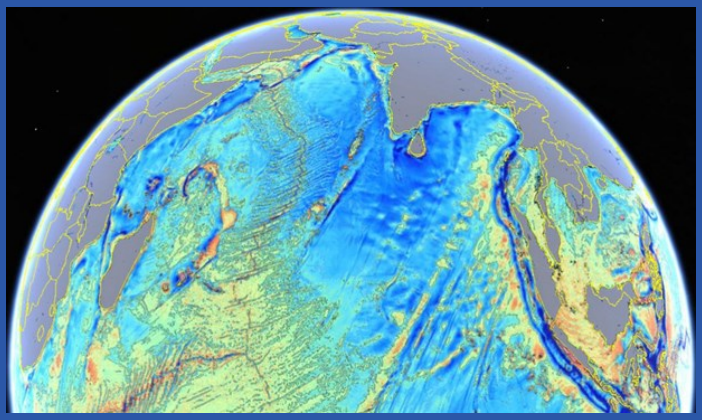

Figure 2: Free-air gravity anomalies depicting geological features of the ocean floor

Geophysical Applications

Satellite altimetry revolutionized our understanding of the shape and structure of the world's sea floor and the geodynamic processes that form it (Fu and Cazenave, 2001). Satellite altimeter data provide an important and definitive confirmation of the theory of plate tectonics which suggest that suggests that the outer most layer of the Earth is fragmented into numerous segments of varying size and the segments called lithosphere which are being moved relative to each other over a fluid substratum (asthenosphere). Spectral analysis of satellite gravity and bathymetry data provided direct measurements of the thickness of the elastic potion of the lithosphere (Elastic Plate thickness). Elastic plate thickness is an important parameter to understand, structure, isostasy and evolution of geological features of the ocean floor (Watts, 2001 and references therein). High resolution marine gravity data from satellite altimeter measurements provided an opportunity to map fine-scale tectonic features such as seamounts, fracture zones, psedofaults on ocean basins carpeted with thick sedimentary cover (Sandwell et al., 2014).

Few case studies demonstrating the applications of satellite altimetry in understanding the structure and evolution of the Indian Ocean is provided below.

The Indian Ocean is youngest in age and smallest in area relative to the other major oceans, Atlantic and Pacific Oceans. But its structure and evolution are very complex and the ocean encompasses with almost all varieties of geological processes. Satellite gravity played an important role understanding the structure and evolution of the Indian Ocean. Fracture zones mapped from high resolution gravity maps were extensively used in paleogeographic models (Eg. Gaina et al., 2009). Geoid and gravity anomaly data of conjugate regions of Bay of Bengal and Enderby Basin provided new constraints on breakup and early spreading history between India and Antarctica (Krishna et al., 2009). Analysis of high resolution satellite gravity of the Arabian and Somali basis lead to the detec-

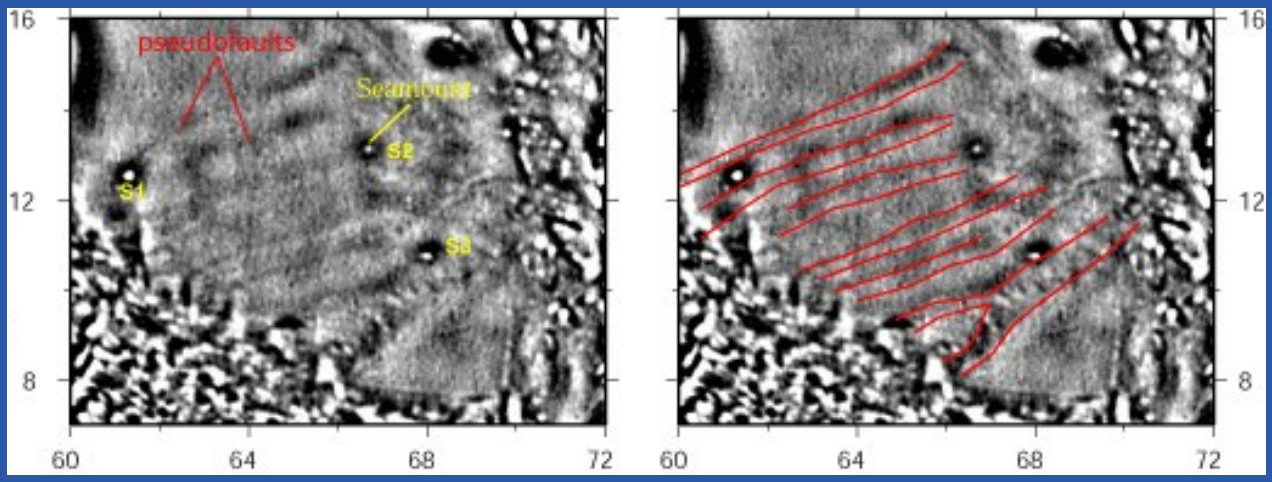

Figure 3: Detection of psedufaults (red lines) and uncharted seamounts (S1-S3) from filtered free-air gravity anomalies of the Arabian basin (Modified after Sreejith et al., 2016).

tion of uncharted seamounts and pseudofaults and thereby provided constraints on the ridge propagation process during the early evolution (Figure 3) of the western Indian Ocean (Sreejith et al., 2016).

Aseismic ridges, formed due to the interaction of mantle plumes with oceanic lithosphere, are known to have played an important role in shaping the oceanic and sedimentary basins in the Indian Ocean. Gravity- bathymetry transfer function analysis provided detailed crustal structure and isostatic compensation of the aseismic ridges of the Indian ocean such as the Ninetyeast Ridge, Chagos-Laccadive Ridge, Laxmi Ridge and 85°E Ridge (Sreejith and Krishna 2013, 2015; Mishra et al., 2017; Rao et al., 2016). Further, Modelling of the geoid and gravity data deciphered the lithosphere-asthenosphere boundary and deep mantle processes beneath Bay of Bengal (Rao et al., 2016).

Ocean State Forecast at SAC: Current Status and way forward

SEEMANTH M, S A BHOWMICK, S RATHEESH, N AGARWAL, R SHARMA and S SHAH

EPSA, Space Applications Centre (ISRO), Ahmedabad

seemanth@sac.isro.gov.in

Accurate prediction of ocean conditions, such as waves, circulation, temperature, mixed layer depth, etc. is very crucial for various activities at the sea, for example naval operations, ship routing, tourism, fisheries, port and harbour construction and offshore industries. Here at SAC, ocean state forecast activity for wave and circulation has been carried out since more than a decade. Satellite data utilization to continuously improve upon these forecasts by means of satellite data assimilation has been one of the major activities of Oceanic Sciences Division at SAC. In order to provide continuous real time forecasts of the three dimensional ocean state, two different models, one is 2-dimensional model for sea surface waves and swell and the other, an ocean general circulation model for entire 3-dimensional physical state of the ocean such as Temperature, salinity, currents, sea level and derived variables such as mixed layer depth, for the are being utilized. These models are specially configured to meet the specific needs of users such as the Navy and the Shipping Corporation of India. The details of these models used are provided below.

Continual advances in the arena of numerical wave modelling have resulted in the community standard third-generation spectral wave models such as WAve Model (WAM), Simulating WAves Nearshore (SWAN) and WAVEWATCH III (WW3). In correspondence to this, a very high resolution data assimilative wave forecasting system based on WW3 model is made operational at SAC. The model set-up is specifically customized of four nested domains including a global (1^0x1^0), Indian Ocean (0.5^0x0.5^0), North Indian Ocean (0.1^0x0.1^0) and a very high resolution coastal (2.5 x 2.5 km) domain covering the entire Exclusive Economic Zone of India. The forecasting system uses 10m analysis and forecast wind components obtained from the National Centre for Medium Range Weather Forecasting (NCMRWF) as the forcing field. The operational wave model runs one time in a day at the 0000 UTC model cycle and start with a 24 hr hindcast for the previous day. Accuracy of wave forecast can be improved by assimilating the wave height measurements obtained from altimeters, on-board different satellites. Real-time application of satellite based observation is one of the major focus area at Indian Space Research Organization (ISRO). In order to improve the predicting capability of the model, significant wave height measurements from SARAL/AltiKa, Jason2 and Jason3 altimeters are assimilated into the model using optimal interpolation technique. The data assimilation module was also installed at Indian National Centre for Ocean Information Services (INCOIS) with their operational wave forecasting system.

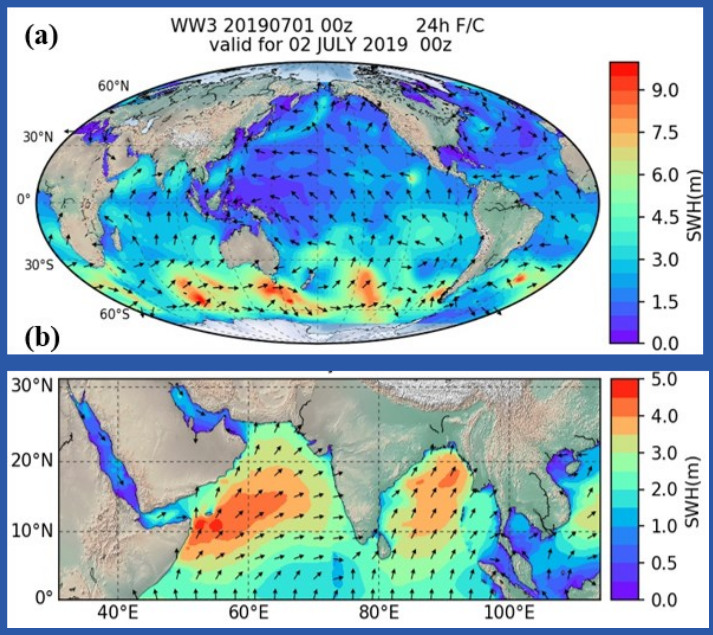

Figure 1: Sample wave forecast from data assimilative wave model at SAC configured for (a) Global (1^0 x 1^0) and (b) North Indian Ocean (0.1^0x0.1^0)

The ocean state forecast parameters such as temperature, salinity, currents, mixed layer depth, sea surface height anomalies are based upon the Modular Ocean Model version 3.0. This is a primitive equation, hydrostatic model with free surface equation. The model is specifically configured for the North Indian ocean (27 ^{0}E — 142 ^{0}E, 35 ^{0}S — 26 ^{0}N) with a variable horizontal resolution such that it is uniform 0.10 x 0.10 in the region 55E – 100E and 10S – 23N and reaching a minimum upto 10 in the rest of the domain. It has 50 levels in the vertical (vertical resolution ranging from 2.5 m at the surface to 5320 m at the bottom, with top 14 levels in the upper 36 m). The vertical mix-

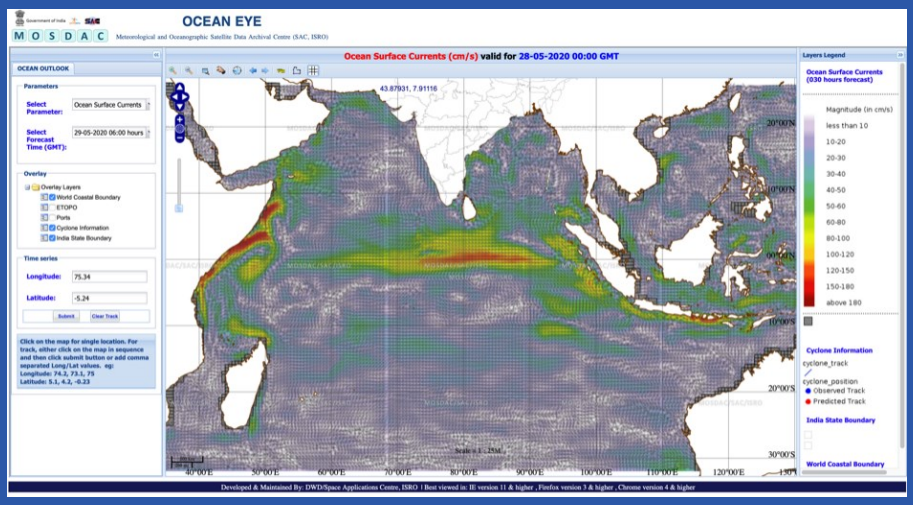

Figure 2: Screenshot of one of the outputs of Ocean Circulation model (currents m/s) disseminated on "Ocean Eye" portal of MOSDAC in real time.

ing based on the scheme of nonlocal K-profile parameterization known as KPP mixing scheme has been used. Bathymetry data is taken from ETOPO-2. Satellite derived diffused attenuation co-efficients are used to determine the shortwave penetration depth. Monthly climatology of altimeter derived river discharge data from Ganga, Brahmaputra (Papa et al., 2010) is used in the model.

The model is forced using the atmospheric fluxes of momentum, heat flux and fresh water fluxes available from NCMRWF. The forecasts are generated for next 120 hours using current days analysis fields at 0000 UTC. In order increase the accuracy of forecasts, satellite derived sea surface temperature and sea level anomaly data are continuously assimilated in near real time. Forecasts of derived parameters such as mixed layer depth, sound velocity, sonic layer depth, tropical cyclone heat potential and ocean mean temperature are also available in real time.

Both these models of wave (except for very high resolution version of 2.5km) and circulation with data assimilation modules have been installed at NODPAC, Kochi and the outputs from these models are disseminated in real time to the naval ships. The outputs from the high resolution wave model that runs at SAC is kept on MOSDAC ftp server for Navy to download. Forecasted wave and circulation parameters such as significant wave height, mean wave direction, mean wave period, swell height, swell direction, temperature, salinity, currents are also disseminated through LIVE MOSDAC (https://live.mosdac.gov.in/) and OCEAN EYE (https://mosdac.gov.in/sci/) for the next 5-days.

In order to forecast ocean biological parameters, work is currently in progress to configure high resolution coupled ocean-biogeochemistry model. This will give the forecast of ocean chlorophyll which is an important parameter used in Potential Fishery Zone (PFZ) detection, especially when the satellite observations are not available due to cloudy conditions. More emphasis is laid on improving upon the accuracy of these forecasting systems by using advanced assimilation techniques and by including more variables for assimilation, such as wave spectrum, vertical temperature and salinity profiles and high resolution imagery from satellites.

Geophysical Parameters in Ocean Biology and Applications using Ocean Colour Monitors

ARVIND SAHAY and R K SARANGI
MED/BPSG/EPSA, Space Applications Centre (ISRO), Ahmedabad
arvindsahay@sac.isro.gov.in

Introduction

Oceans occupy almost 70% of the surface of our planet Earth. To observe, explore, monitor and manage our vast oceans, satellites are wonderful tools, since it gives synoptic coverage and ideal repeativity/revisit of the vast oceans. The colour of ocean is not just blue or green but it depends on the type of substances present in the ocean water. The main substances that present in ocean water are phytoplankton (tiny floating plants in ocean water), total suspended matter and dissolved/detrital matter and the optically active constituents present in these substances are chl-a pigment (phytoplankton), inorganic suspended particles (total suspended matter) and dissolved and particulate organic carbon (dissolved/detrital matter). These constituents/parameters play an important role in biological oceanographic studies of the ocean waters. These constituents can be detected from space through their distinct optical properties in the optical region of electromagnetic spectrum using Ocean Colour Monitors (OCM). Ocean Colour Monitors are passive radiometers, which detect reflected Sun light in the optical region of electromagnetic spectrum coming from the surface of ocean waters. This reflected light from the surface of water carries information about the water constituents and is used in estimating ocean colour geophysical parameters.

Ocean color satellite missions and its perspective

The ocean colour study was initiated using the Landsat satellite data in 1970s. Then exclusively the NIMBUS-Coastal Zone Colour Scanner (CZCS) mission started in 1978 and continued successfully until 1986. Later on, in 1990s ocean colour remote sensing started with improved sensor based satellite missions like Indo-German Collaboration IRS-P3 MOS, NASA's Sea viewing Wide-Field of View (SeaWiFS), Japan's OCTS and Indian's Ocean Colour Monitor-1 (OCM-1 onboard Oceansat-1, the first exclusive ocean colour satellite of India along with microwave radiometer MSMR in 1999). In next decade, the major ongoing ocean colour missions were the NASA's Moderate Resolution Imaging Spectro-radiometer (MODIS in 2002), MERIS of ESA (2002) and OCM-2 (onboard Ocenasat-2, launched on September 23, 2009 by India). Another generation of ocean colour instruments was launched into polar orbit in 2011, named Visible Imaging Infrared Radiometer Suite (VIIRS) by Suomi National Polar Orbiting Partnership (NPP) spacecraft. All these satellites comprise of Ocean Colour Monitor (OCM) instruments that provides Top of Atmospheric (TOA) radiance emanating from water surface after passing through the atmosphere. TOA radiance is used in deriving geophysical parameters for ocean biology studies. There has been planned schedule for the launching of Oceansat-3 comprising OCM, SSTM and Scatterometer by our National Space Agency ISRO during mid of 2020.

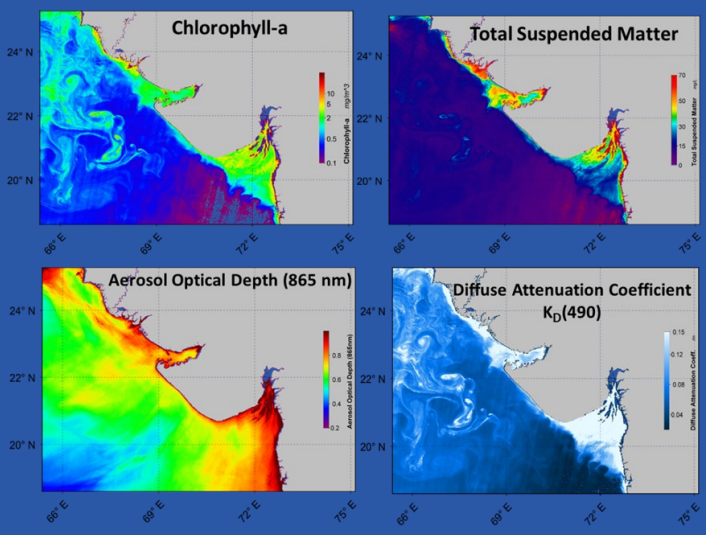

Figure 1: Geophysical parameters derived from Ocean Colour Monitor of Indian Oceanographic Satellite (Oceansat-2, OCM) used in Ocean Biology.

Geophysical parameters retrieval from Ocean Colour Sensors

The ocean colour geophysical parameters can be used in algal blooms monitoring, cyclone and dust induced productivity, upwelling processes, biogeochemical cycle of ocean waters, sequestration of carbon, fixation of nitrogen and atmospheric aerosol studies. The important geophysical parameters that can be detected through OCM are chlorophyll-a, total suspended matter, aerosol optical depth, diffuse attenuation coefficient, etc. are shown in figure-1.

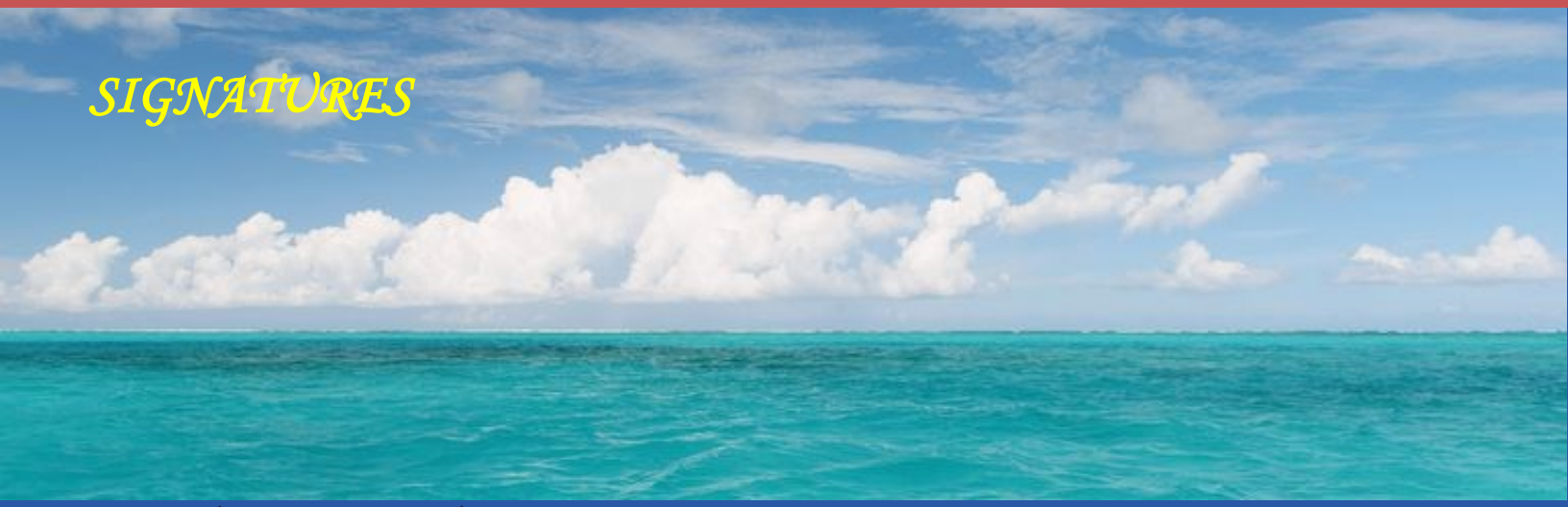

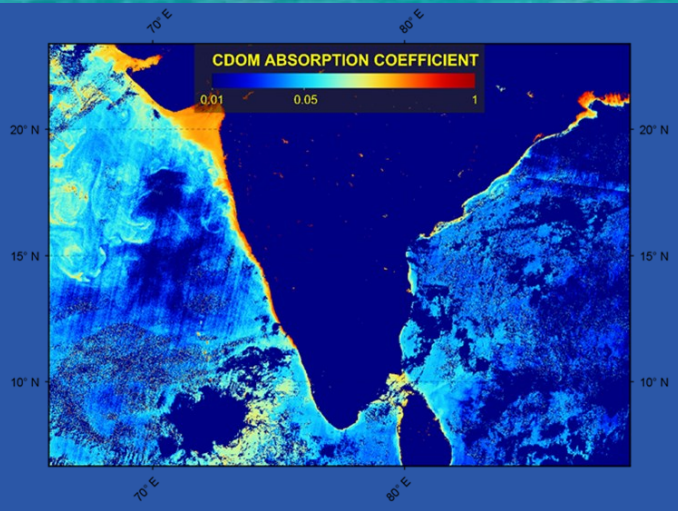

Figure 2: CDOM distribution map using Oceansat-2, OCM in Arabian Sea and Bay of Bengal waters

CDOM absorbs over 90% of total UV radiation entering the euphotic layer, thereby serving a photo protective role in biological processes. CDOM provides UV protection with absorption of harmful UV-B and UV-A radiation in the water column. UV absorption by CDOM produces a set of photochemical reactions at the sea surface including release of CO_2, CO and transformation of microbial bioavailability of organic matter. In CDOM-rich waters, absorption of blue wavelengths causes rapid attenuation of light and a spectral shift to orange and red wavelengths. It is an important component, which indirectly influences the climate change by the biogeochemistry of carbon and Sulphur cycles. The above geophysical parameters can be derived using ocean colour instruments from space-borne platform or satellites. These are very important for studying marine ecosystem and marine environment in global oceans and control ocean biology and various oceanographic processes.

Applications of ocean colour monitor datasets

Satellite ocean colour and the derived data has been utilized for the purpose of quantifying ocean carbon flux, i.e. the primary productivity study, ocean biology and upper ocean processes, coastal processes including the sediment transport, identifying potential fishing zones, algal bloom studies, etc. on a regular basis.

Ocean carbon flux

The principal users of satellite-derived ocean-basin to global-scale phytoplankton chlorophyll fields are the global-change programs. These programs need long term data sets, including satellite data sets, to quantify the effects of periodic climate phenomena such as *El Nino*, and to separate the periodic effects from those that may be occurring in response to human-induced changes to the ocean environment, including permanent climate changes (IOCCG, 2000). Biological processes affect net air-sea CO_2 fluxes in two fundamental ways. First, photosynthesis removes CO_2 from surface waters and transforms it into organic carbon, initially bound within phytoplankton (microscopic plants) and other particles. Second, a large percentage of organic particles formed within surface waters eventually sink through the main ocean thermocline. Satellite ocean-colour sensors are now the standard tool to determine ocean-basin to global distributions of phytoplankton chlorophyll-a. Ocean primary production (CO_2 uptake by plants) cannot be directly measured from space, but is calculated from chlorophyll-a concentration. Model studies show that global productivity calculations are very sensitive to the input surface chlorophyll fields (Platt and Sathyendranath, 1988, Wernand et al, 2013)) and thus satellite ocean-colour imagery is very important for accurate calculations of the mean and time-varying components of the global distribution of ocean primary production and new production with the retrieval of nutrients and uptakes.

Ocean biology and upper ocean processes

Phytoplankton and other particles absorb heat in the upper ocean, which in some circumstances can be important term in ocean heat budgets. Ocean-colour images are being used in upper ocean heat flux calculations. In regions such as the Arabian Sea (Sathyendranath *et al.*, 1991) and the Equatorial Pacific, this approach makes a significant difference to the computed heat flux, as well as the vertical distribution of heat in the upper ocean. Ocean colour imagery is the only source of biological information routinely available on a global basis and is thus one of the few sources of information that can be used to validate

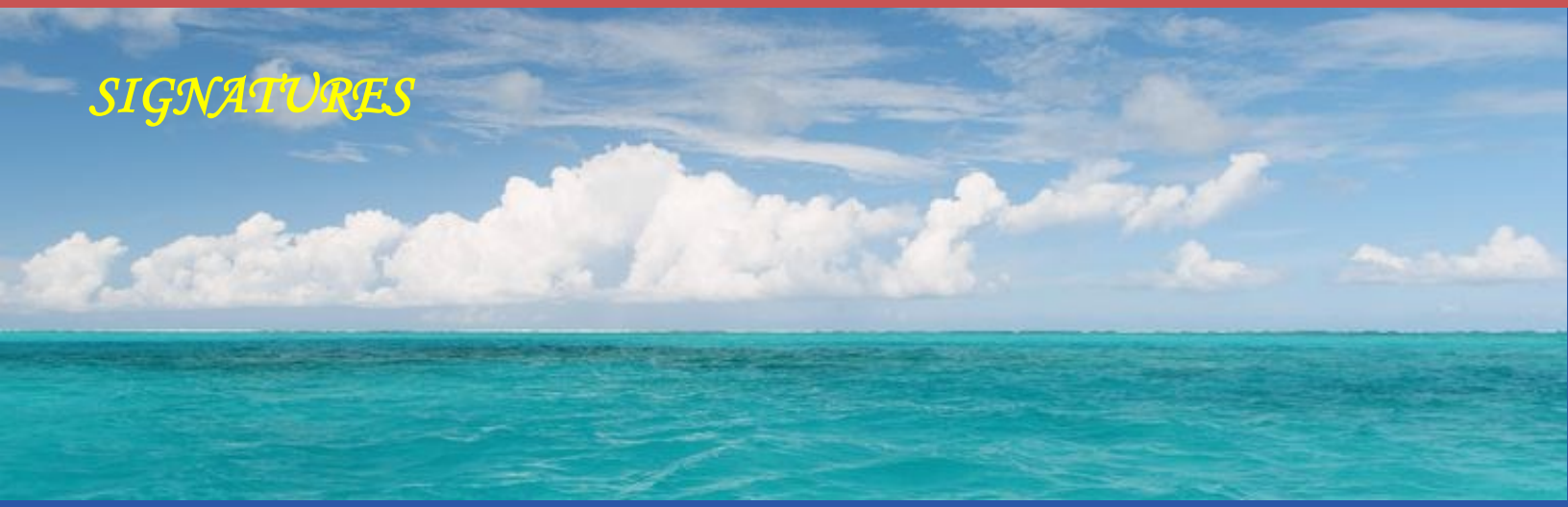

phytoplankton distributions predicted by the regional to global scale numerical models.

Coastal processes

Erosion or modification of the shoreline is often associated with changes in the sediment load of the water column, which is redistributed from one place to another or derived directly from river run-off. In India, in many bays, estuaries, and seas, a large proportion of pollutants come not only from coastal sources such as dumping, industrial and municipal discharge (point sources) but also from watershed (non-point source). Among the many upstream activities known to degrade water quality in coastal areas are logging, agriculture, dam building for power and irrigation, urbanization, etc. Remote sensing can detect turbidity (suspended sediments) and colour (chlorophyll), yellow substance (gelbstoff/gelvin) which are indicators of water quality. Chlorophyll indicates trophic status, nutrient load and possibly presence of man-made pollutants in the coastal waters. Suspended sediments affect navigation, fisheries, aquatic life, recreational potential of sea resorts. They also carry absorbed chemicals. Any pollutant having distinct colour or turbidity can be identified. The ocean colour data becomes extremely useful in monitoring the water quality in operational mode.

Detection and monitoring of phytoplankton bloom

Phytoplankton blooms may affect fisheries and play important role in fixation of nitrogen. Occasionally these algae grow very fast or “bloom” and accumulate into dense, visible patches near the surface of the water. Blooms of plant origin are known to occur under various conditions in the inshore regions. These may take place, often with cyclical regularity in any particular area when some optimum conditions of temperature, salinity, sunlight, nutrients, etc. prevail in the marine environment. The bloom usually takes place rather suddenly and spreads, sometimes changing the colour of the surface waters into red, green, brown, yellow and hay colour (IOCCG, 2000). This modifies the optical properties of water thus enabling the detection of blooms through remote sensing. Knowledge of presence, absence and timing of elevated plant concentrations is a prerequisite for successful planning of studies of plant productivity, the investigation of suspension feeding zooplankton and the seasonality of particle fluxes to the deep sea (Banse, 1987). The blooms can form rapidly and it is often difficult to assess their development and extent from traditional sampling methods using boat or fixed site monitoring station. Remote sensing techniques offer a practical additional tool in overcoming these problems (Zibordi *et al,* 1990). Spectral characteristics of particular pigments within algal bloom cells has become possible to detect the bloom types.

Fishery information

The capabilities of satellite remote sensing technology, combined with conventional data collection techniques, provide powerful tool for the efficient, cost effective management of marine living resources. Recent advances in data acquisition systems, analysis methods and communication technologies have prompted the use of satellite data in the field of fisheries for both near-real-time support of the day-to-day fishing activities, and in the analysis of decadal trends in fish populations (Caraux and Austin, 1983). Satellite remote sensing applications in fisheries have concentrated on the measurements of ocean temperature and colour and computation of ocean transport based on satellite measured wind stress. Synoptic estimates of chlorophyll are important because phytoplankton variability in space and time controls the marine environment and all animals rely on phytoplankton for food. Information on the changing ocean colour, rather than on average ocean conditions, is necessary to understand and eventually to model the efforts of ocean environment on fish stocks.

Summary

Ocean colour data has been used for various oceanographic research and operational activities. The type of research activity generally determines the type of data that will be most useful to researchers and operational agencies. However, our knowledge on our oceans is limited. Ships, coastlines, and islands provide places from which we can observe sample, and study small portions of oceans. Different colours reveal the presence and concentration of phytoplankton, suspended sediments and dissolved organic chemicals in ocean. Thus, looking at the colour of an area of the ocean that allows us to estimate the amount and general type of phytoplankton in that area, and tells us about the health and chemistry of the ocean. Compar-

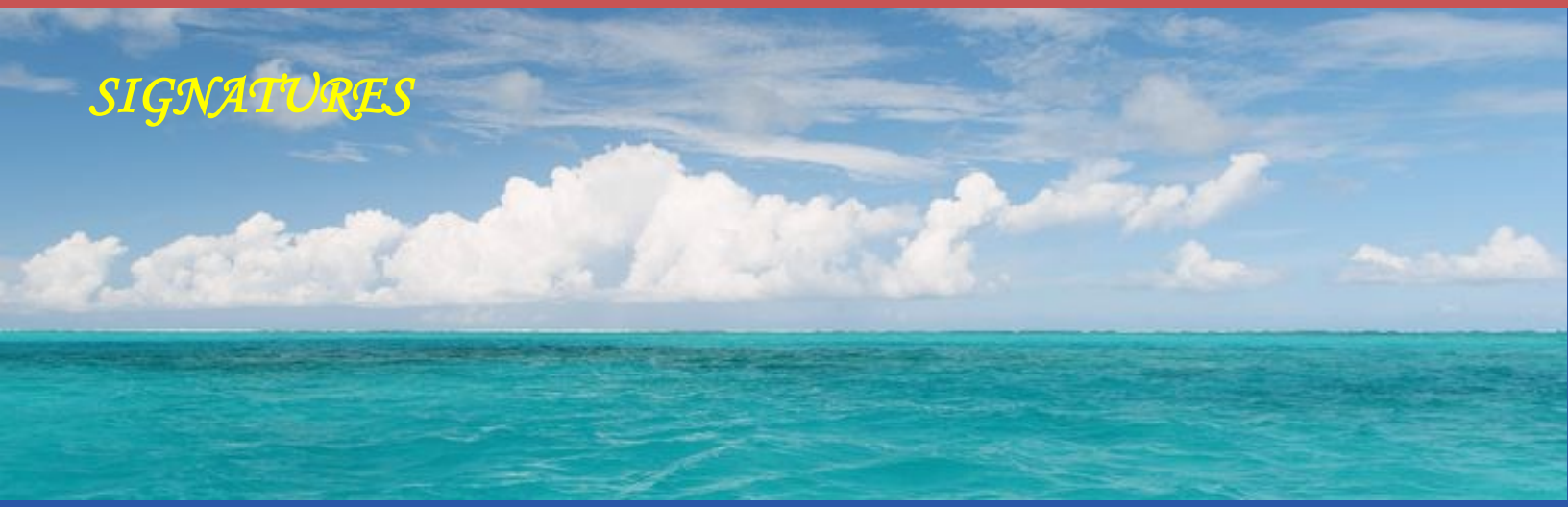

ing images taken at different time periods and in sequences tell us about changes that occur. The spectral and radiometric resolution of ocean colour sensors and respective channels play the crucial role in accurate estimation of geophysical parameters. The phytoplankton and other associated particles are of course very important. These small plants are the beginning of the food chain in major portion of the planet. As phytoplankton grow and multiply, small fish and other animals eat them as food as part of food chain and food web. The ocean fishing industry finds good fishing spots by looking at ocean colour images to locate areas rich in phytoplankton. In addition, satellite ocean-colour imagery has become important for accurate calculations of the mean and time-varying components of the global distribution of ocean primary production and new production due to nutrients. Hence, the ocean colour studies, geophysical parameters retrieval with justified accuracy (with timely calibration and validation process) and research and applications are on the frontier stage to monitor the global oceans in synoptic manner.

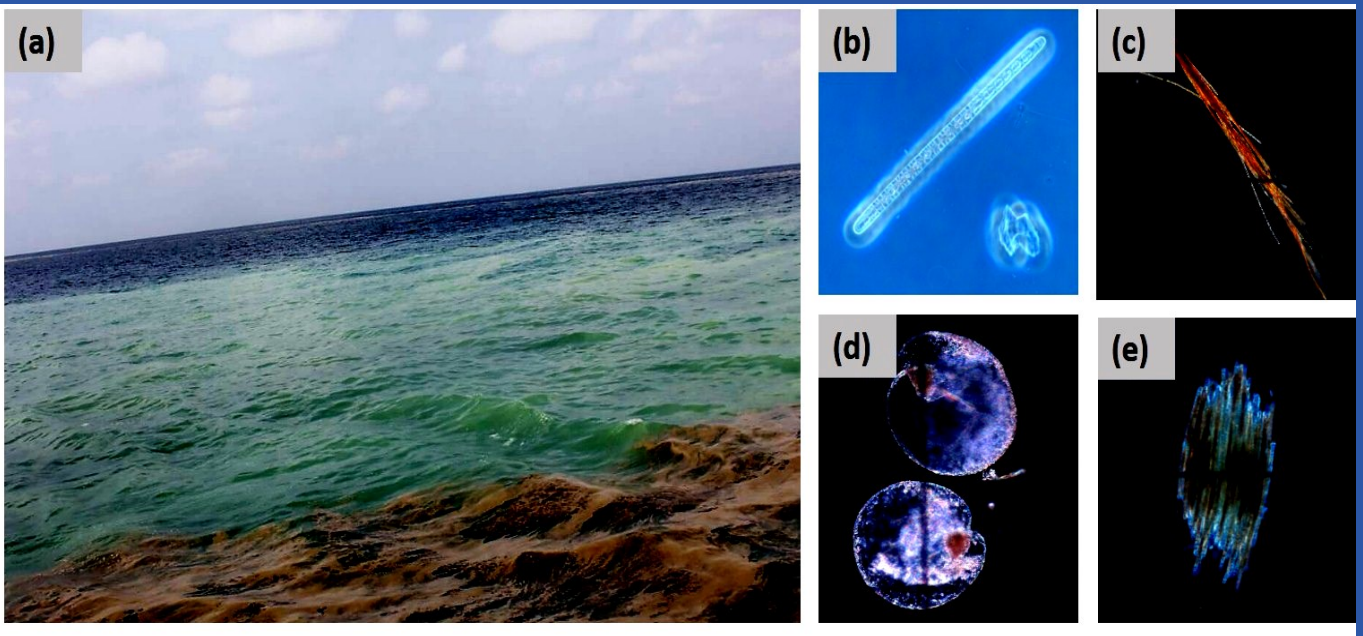

(a) Trichodesmium bloom in Arabian Sea (b) Trichome single cell
(b) (c) Trichome colony (d) Noctiluca cell (e) Trichome colony

Courtesy: Ms. Anima Tirkey, MED/BPSG/EPSA
Sagar Sampda-359

Cyclone induced surge & Coastal Inundation

ANUP KUMAR MANDAL
OSD/AOSG/EPSA, Space Applications Centre (ISRO), Ahmedabad
anupmandal@sac.isro.gov.in

Accurate prediction of storm surge and coastal inundation is very crucial in disaster management during a cyclone. Storm surge induced coastal inundation is typically considered as the worst disaster due to the cyclone, which accounts for an estimated 90% of cyclone-attributable mortality. Although, the Northern Indian Ocean (NIO) only accounts for 7% of global tropical cyclones, the tropical cyclones along the Bay of Bengal alone accounts for 60% of all deaths due to storm surge.

Numerical storm surge modelling is the approach for early warning during cyclogenesis. However, the accuracy of storm surge forecast depends on accurate numerical weather prediction (NWP) model wind forecasts as well as the proper representation of coastal geometry. Forecasting of storm surge during a cyclone has been made operational at Space Applications centre. Currently state of the art Advanced Circulation (ADCIRC) model coupled Simulating Waves Near Shore (SWAN) model has been used with NCMRWF forecast wind forcing at 0.25° spatial resolution. The operation mesh that has been used to simulate storm surge operationally has a resolution of 1km near coast and 50km in the open ocean. The operational output of storm surge for Fani cyclone (2019) is shown in Figure 1(a).

Coastal inundation forecast is most important during the landfall of a cyclone. Therefore, at present coastal inundation forecast is generated from 72 hours' prior landfall. Forecasting coastal inundation requires very high resolution and accurate representation of the domain. Small creeks and rivers act as feeders which carries the storm surge inland, often enhancing the surge height and inducing devastating effects towards the inland. So, in order to achieve a realistic coastal inundation, very high resolution representation of the geometry is required especially along the coast, which can capture the creeks, rivulets and lakes adjoining the coastal area. Forecasting cyclone induced coastal inundation along the East coast of India has been made operational using same ADCIRC+SWAN model but using a higher resolution mesh.

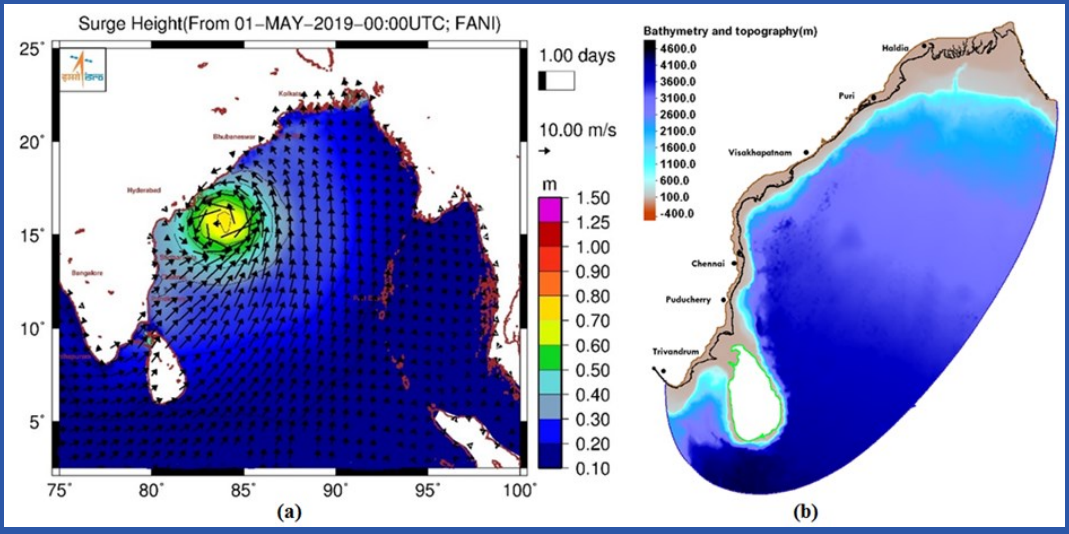

Figure 1: (a) Storm surge forecast during FANI cyclone (b) Inundation mesh for coastal inundation forecast

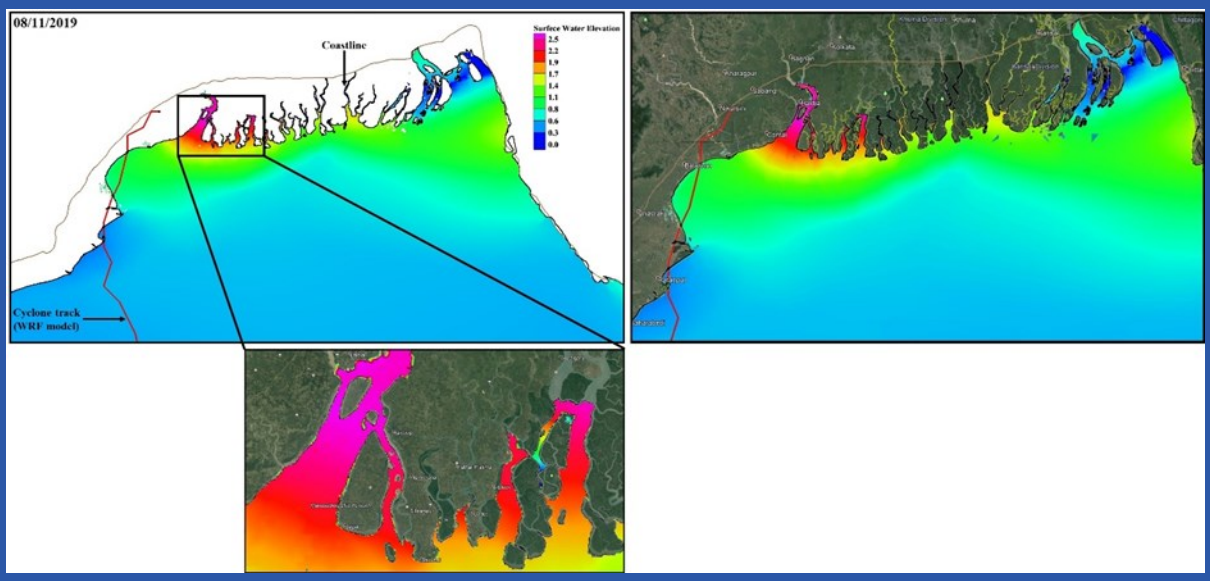

Figure 2: Storm tide during Bulbul cyclone (1 day prior to landfall)

Therefore, less resource and time is needed to simulate inundation than storm surge only. Bathymetry of the domain is prepared by integrating digital coastal bathymetric chart with global digital elevation model (DEM) ETOPO-2 and the topography of the land region is created by merging fine resolution airborne DEM (ALTM-DEM) with CARTOSAT-2 DEM and Shuttle Radar Topography Mission (SRTM) DEM. The operational mesh prepared from the merged datasets is shown in Figure 1(b), which has a very high spatial resolution of 100m near coast. The Weather Research and forecasting (WRF) model forecast winds at 5km spatial resolution are used as the primary forcing parameter for forecasting coastal inundation.

The forecasted storm tide and associated coastal inundation is shown in Figure 2 for Bulbul cyclone (2019). Both storm surge and inundation products are available at https://mosdac.gov.in/scorpio1/.

Detection of OIL-SPILL and its trajectory forecasting

ADITYA CHAUDHARY[1] and RATHEESH RAMAKRISHNAN[2]
[1]OSD/AOSG/EPSA, [2]GSD/GHCAG/EPSA, Space Applications Centre (ISRO), Ahmedabad
aditya.osd@sac.isro.gov.in

Oil Spill events over the oceans have been considered as a concern for the scientific as well as disaster management authorities. Both natural as well as anthropogenic oil spills are observed over the oceans. Natural oil spills occur due to leakages through fractures and sediments of the underwater rocks. Anthropogenic oil spill sources include the accidents occurring over the offshore oil rigs, accidents of the vessels containing the crude oils, leakage and illegal discharge of oil from the ships on the major shipping routes and lanes which transport the crude oil. Oil spills have a potential to cause severe damages to the marine ecosystems by polluting the surface as well as subsurface of the ocean. The release of the crude oil in the open ocean can cause petroleum toxicity and also can deplete the oxygen content in the ocean thus causing a havoc on the marine ecosystems. Effects of the oil spills can be felt for months as the oil spills can form the tar balls and get deposited over the beaches. When oil spills reach near the coasts where the human population resides then it creates extensive damage to fishing and tourism. It takes a lot of effort for cleanup and restoration activity at the beaches and the coastal areas of the areas affected by the oil spills. More the amount of oil spilled more is the damage caused.

In the recent decades, remote sensing has played a pivotal role in monitoring oil spill events. For large scale observations the space-borne sensors offers to provide unprecedented observations of the oil spill events. Space borne sensor include the high resolution Optical as well as the Synthetic Aperture Radars (SAR). When the remote sensing observations are available the oil spills can also be forecasted based on the physics of the dispersion of the oil spills. The sea surface currents, sea surface winds, tides, wave induced drift, oil type are the most important in determining the dynamics of the oil spills. High resolution models model currents, tidal current models, wave models and numerical weather forecast winds can be used to forecast the oil spill trajectories. In the recent years, lagrangian technique based approach (tracking the particle) which takes the advantages of recent developments

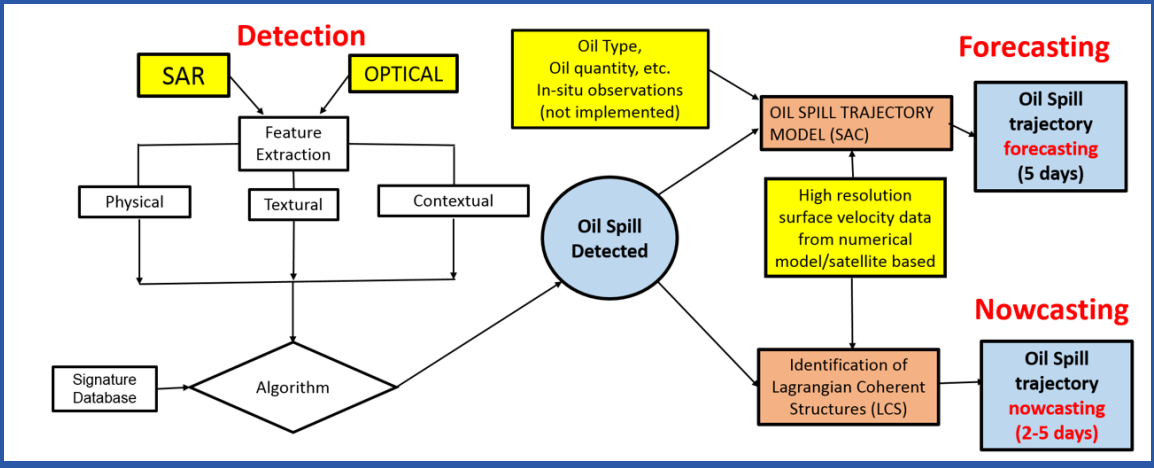

Figure 1: *Flow chart showing detection of oil spill, nowcasting and forecasting of the oil spill trajectory.*

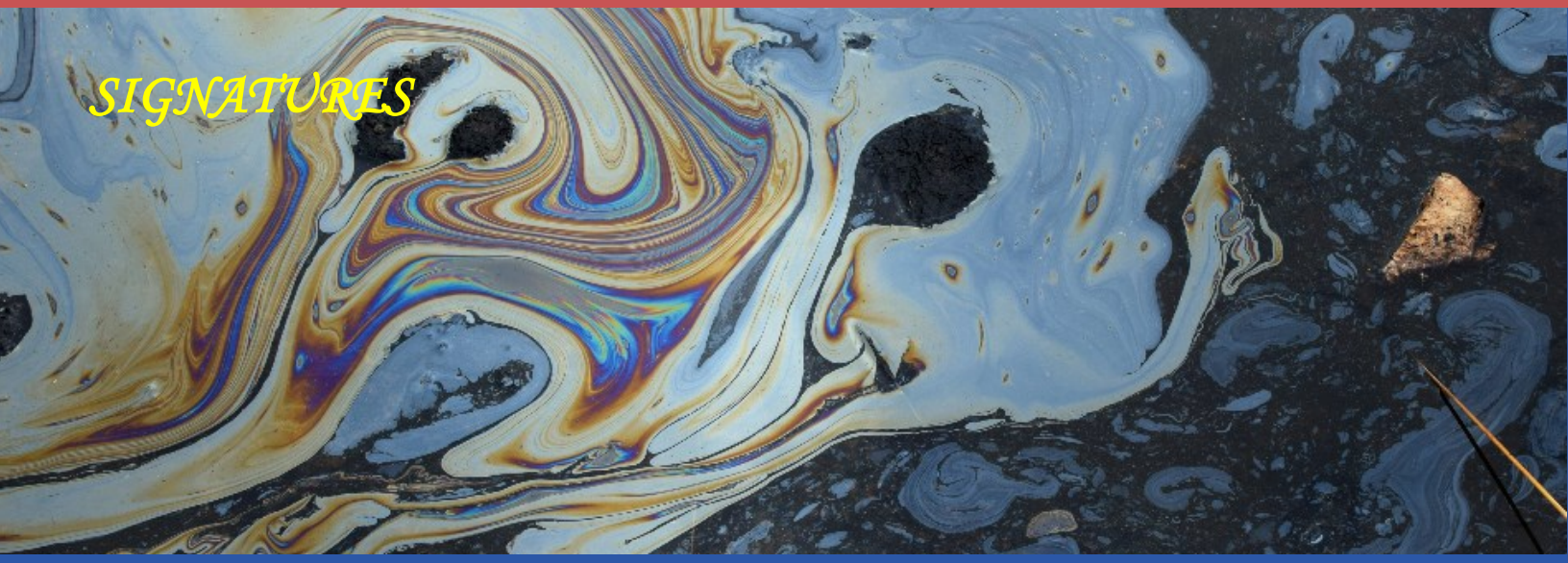

One of the recent oil spill case reported near the Indian coastal region is the Chennai oil spill case which happened at 28 January 2017. It was reported to be caused due to collision of the ship vessels and released a significant amount of the oil in the sea near the Kamarajar Port (Ennore port). Various news channels covered the event and the beaches were said to effect by the oil spill event. The cleanup process took months to fully clean the beaches. The SAR image was able to detect the oil spill. The following subsection provide the analysis of this oil spill event. Sentinel-1 SAR data acquired on 29 January 2017 in IW mode, subsuming the Chennai coastal region is downloaded and is used to detect the oil spill region (Figure 2(a)). VV polarised data is used for the analysis. Auto Segmented Image using the fuzzy logic technique is shown in Figure 2(b). The detection algorithm was able to differentiate oil spill from the biogenic slicks Figure 2(c).

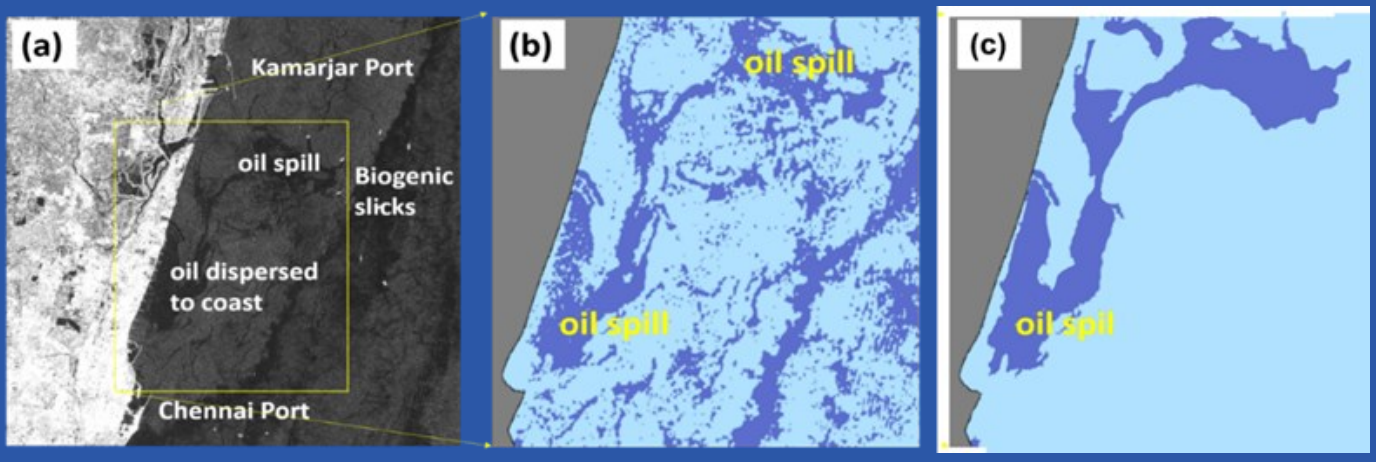

Figure 2: (a) is Image from Sentinal SAR at the Chennai Coast as obtained on 29 January 2017. (b) is the segmented image to detect dark region (c) classification of dark region as oil spill

A simulation was performed by using oil spill detected using Sentinel-1 SAR images as initial condition using the numerically forecasted currents, wind, waves and tides. The simulations are shown for various time steps in Figure 3. The simulation ended within 1 day of the initialization. Southward movement of the oil spill was observed. This was validated with the ground reports..

The LCS based analysis using the altimeter currents was also used for nowcasting this oil spill. We have used the altimeter currents and applied the date 28 January 2018 (with backward integration time T=15 days). The sequence of images (in Figure 4) from 28 January 2017 to 2 February 2017 shows the dominant attracting regions in black. Red arrows show the LCS core regions. We can figure out that near the Kamarajar port (near where the accident happened) no consistent LCS core are found. One problem we can also figure out is that because of its closeness to the coast the altimeter currents are not valid. LCS attracting/converging regions are observed parallel near to the coast, which makes the oil to get dispersed along the coast. The movement of the oil is restricted due to the presence of along shore LCS attracting/converging region.

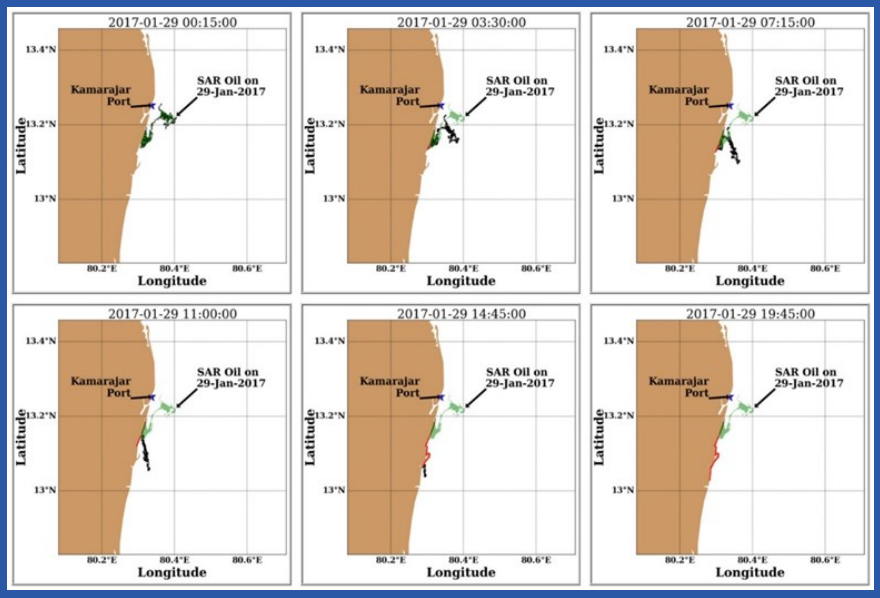

Figure 3: Sequence of images showing the simulation of the Chennai oil January 2017 using the SAR detected oil spill patch. Red color represents the beached oil. Green patch is the oil spill observed from SAR image on 29 January 2017.

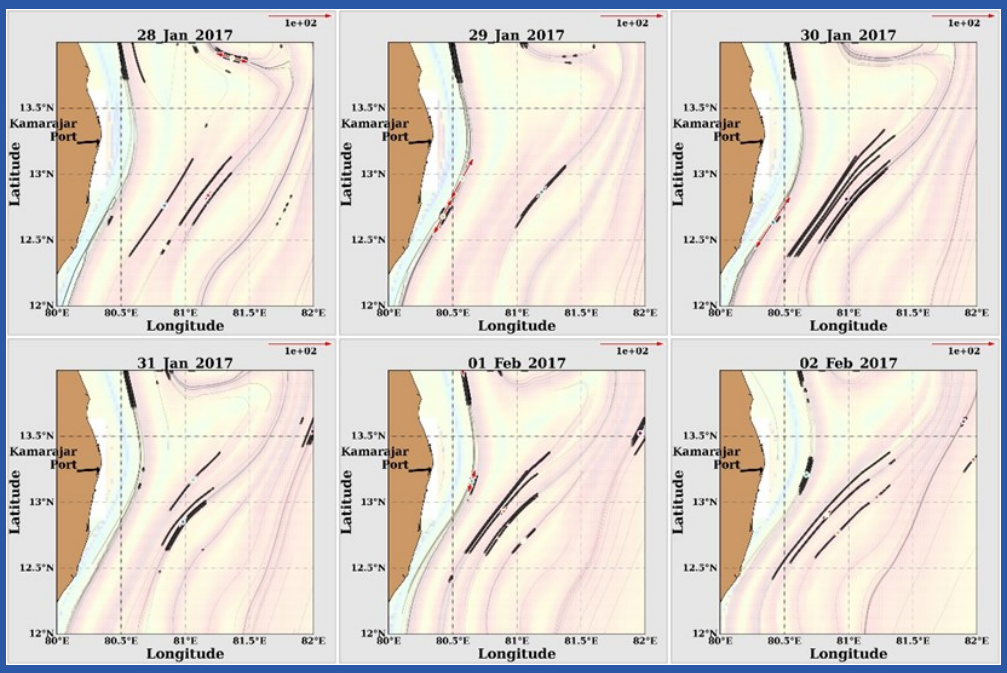

Figure 4: LCS segments with strong attraction are shown in black segments, red arrows show the LCS cores from altimeter derived currents. Background is the Finite time lyapunov exponent field.

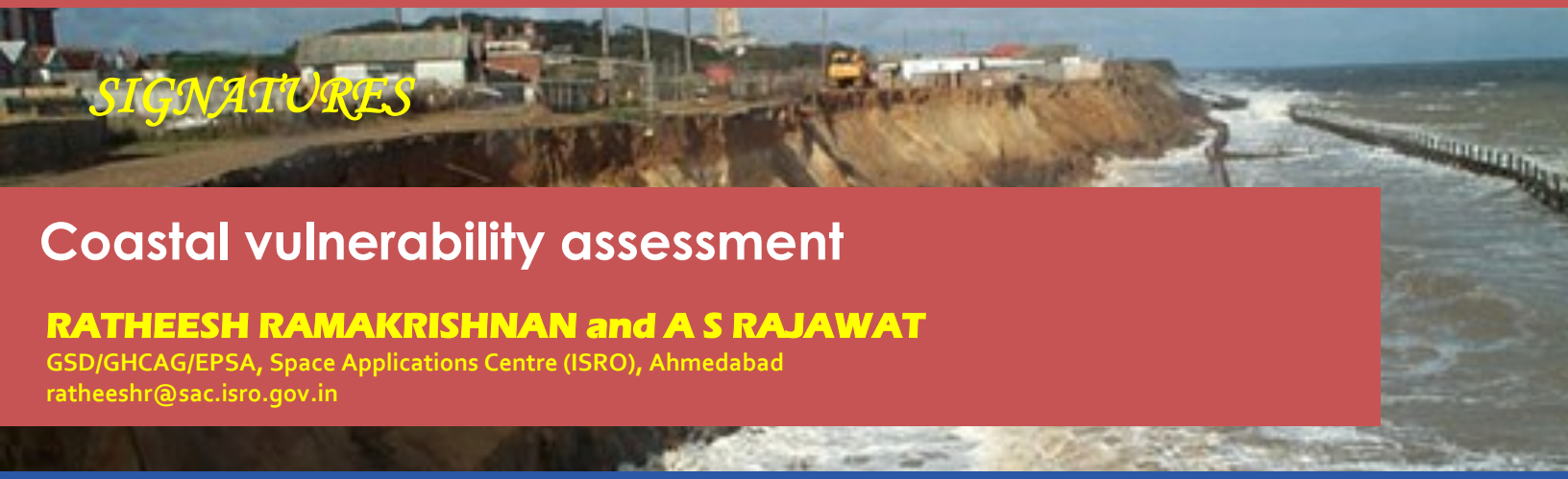

Coastal vulnerability assessment

RATHEESH RAMAKRISHNAN and A S RAJAWAT
GSD/GHCAG/EPSA, Space Applications Centre (ISRO), Ahmedabad
ratheeshr@sac.isro.gov.in

Assessing the preparedness of the coastal region to any natural hazard is a major task among the coastal management authority, where identification of relative vulnerable of coast is a prime concern. Anticipated sea level rise (SLR), storm surge during cyclone, tsunami are the major natural hazards that have a direct impact to the coastal region. Assessment of coastal vulnerability for different coasts are demonstrated that have primarily used the integration of physical variables and socio-economic conditions of the study region. The coast is segmented to various risk categories, namely; low-, moderate-, high- and very high. Various techniques are used to estimate the coastal vulnerability index (CVI). CVI is estimated for Andhra Pradesh due to SLR by integrating differentially weighted rank values of five physical variables, namely coastal geomorphology, coastal slope, shoreline change, mean spring tide range and significant wave height. At Saurashtra coast, Total Vulnerability Index is estimated based on Exposure Index, Sensitivity Index, and Adaptive Capacity Index. Analytical Hierarchical Processes (AHP) is used to estimate the Integrated Coastal Vulnerability Index (ICVI) from the Physical Vulnerability Index (PVI) and Social Vulnerability Index (SVI). CVI provides valuable information on the degree of potential vulnerability risk which serves as a guide to develop adaptation measures by the coastal zone management authority.

Introduction

Urbanisation and rapid growth of coastal cities have been the trend over the last few decades, leading to numerous mega cities around the world facing diverse coastal hazards. One of the major hazards for the coastal region is sea level rise (SLR), which can lead to permanent loss of valuable land, property and natural resources along the coastal region. Climate change, associated sea level rise and impact on the coastal zone are current issues of global magnitude and concern. Global warming and the resulting climate change and sea level rise have increased the anxiety among the people about their immediate future. The global warming in the past century was estimated to be 0.8°C; the rise in temperature in the past three decades alone was 0.6°C at the rate of 0.2°C per decade (Hansen et al. 2006). The ramifications of global warming both in physical and biological world, by and large, reflect the impact of greenhouse gases. Arctic ice sheet is rapidly retreating and if this trend continues the polar bear population would decrease by two-thirds by the midcentury (Courtland 2008). Comparing the altitudinal distribution of 171 forest plant species between 1905 and 1985, and 1986 and 2005 along the entire elevation range up to 2,600 m above sea level, Lenoir et al. (2008) observed that the climate warming has resulted in a significant upward shift in species optimum elevation averaging 29 m per decade.

The most commonly accepted impact of global warming is the eustatic rise in sea level (Allan and Komar 2006) due to thermal expansion of seawater and the addition of ice-melt water. The direct impact of sea level rise would be in the coastal zone, which are low lying and are highly resourceful and densely populated. The SLR will induce an accelerated erosion and shoreline retreat due to increase wave strength as water depth increases near the shore, besides leading to saltwater into coastal groundwater aquifer, inundation of wetlands and estuaries, and threatening historic and cultural resources as well as infrastructure (Pendleton et al. 2004).

Storm surge is considered one of the significant threats to coastal community (Santos et al. 2013). It is predicted that with the climate change-induced global warming and sea-level rise, coastal flood risks are likely to increase over the upcoming future due to increasing storm intensity, accelerating sea-level rise and land subsidence. Furthermore, Knutson et al. (2010) predicted that at the end of the twenty-first

century, there will probably be fewer, but stronger storms globally. Small and Nicholls (2003) estimated that about 23% of the world's population live within 100 km from the coast, and this number is likely to increase to 50% by 2030. According to Peduzzi et al. (2012), coastal populations are becoming more prone to extreme flooding from tropical cyclones.

Another major hazards due to anthropogenic influences is coastal erosion, which leads to permanent loss of valuable land, property and natural resources along the coastal region. The shorelines are dynamic as they change spatially and temporally in response to variations in coastal processes induced either naturally or anthropogenic. Shoreline change rate is one of the most common measurements used by coastal scientists, engineers and land planners to indicate the dynamics and the hazards of the coast. Coastal erosion is considered as a major threat worldwide. Indian shoreline on the either side of its peninsula is subjected to erosion in varied strengths (Rajawat et al. 2015).

Development of coastal vulnerability index for Andhra Pradesh coast (Rao et al., 2009)

The east coast of India bordering the Bay of Bengal is a passive continental margin developed during separation of India from Antarctica in the Late Jurassic. Administratively, the 2,350-km-long east coast forms the eastern seaboard of three States—Orissa in the north, Andhra Pradesh (AP) in the centre, and Tamil Nadu in the south (Fig. 1). AP coast is 1030 km in length, including the 300-km-long Krishna– Godavari delta front dominating its central part. The coastal sector north of these deltas is characterized by headland-bay configuration with a number of rock promontories jutting into the sea, especially over a 185-km stretch on both sides of Visakhapatnam city (inset B in Fig. 1). The Penner delta and Pulicat Lake are the dominant features along the coast south of the Krishna–Godavari delta region. The region is densely populated with more than 6.5 million people living within 5-m-elevation above the sea level including the port cities of Visakhapatnam, Kakinada and Machilipatnam. The AP coast is known for frequent tropical cyclones and associated floods and tidal surges causing loss of life and property in the region. The future sea-level rise is likely to further intensify the storm surges, besides accelerating shoreline erosion and other problems like seawater intrusion and damage to coastal structures, thereby making the AP coast much more vulnerable in future. In this background, a coastal vulnerability assessment is made aimed to identify the degree of vulnerability of different coastal segments of AP.

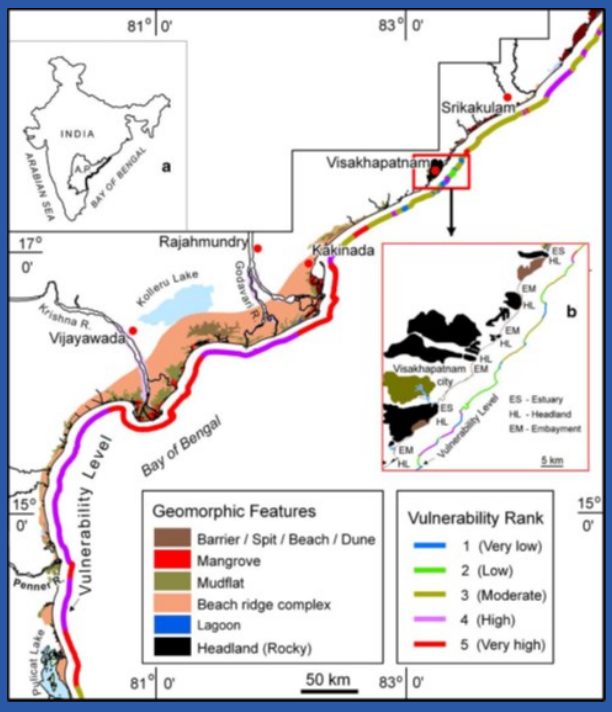

Figure 1: Geomorphology of the AP coast up to ~5 m elevation. The thick colored parallel line, indicates the vulnerability ranking on the relative resistance of the geomorphic features that fringe the coast

Five physical variables of the AP coast are used to measure the coastal vulnerability. They are (1) coastal geomorphology, (2) coastal slope, (3) shoreline change (erosion and accretion during a 16-year period between 1990 and 2006), (4) mean spring tide range, and (5) significant wave height. Depending up on the nature of each of these variables, the entire AP coast is segmented and assigned vulnerability ranks ranging from 1 to 5, with rank 1 representing very low vulnerability and rank 5 indicating very high vulnerability as shown in the table 1. Applying the classification based on table 1 all the coastal sectors along the AP coast are ranked from one to five as depicted in figure 2.

Table 1 Coastal vulnerability classification based on the five physical variables

Variable	Coastal vulnerability rank				
	Very low (1)	Low (2)	Moderate (3)	High (4)	Very high (5)
Geomorphology	Rocky coasts	Embayed/ indented coasts	Beach ridges; high dunes (>3m) vegetated	Low fore dunes (<3 m); estuaries; lagoons	Mudflats; mangroves; beaches; barriers/spits
Coastal slope (%)	>1.00	0.50-1.00	0.10-0.50	0.05-0.10	<0.05
Shoreline change	Accretion >5.0	Accretion <5.0	Nil	Erosion <5.0	Erosion >5.0
Mean spring tide	< 1.0	1.0-2.0	2.0-4.0	4.0-6.0	>6.0
Significant wave	<0.55	0.55-0.85	0.85-1.05	1.05-1.25	>1.25

All the five maps showing the coastline segmented according to their vulnerability ranks are then combined in GIS to derive a coastal vulnerability index (CVI) for various segments of the entire coast. Relative ranking is assigned to various coastal segments based on the vulnerability level in terms of each of the five parameters considered in the study. Considering the relative significance of geomorphology and slope over the rest of the three variables in deciding the coastal response to sea-level rise, a maximum weightage of 4 is assigned to these two variables.

$$CVI = 4g+4s+4c+t+w$$

Where g refers to vulnerability ranking of geomorphology of the coastal segment in question, s refers to that of coastal slope, c to that of shoreline change, t refers to spring tide range and w refers to the vulnerability rank of the significant wave height. The numbers 4 and 2 are the arbitrary weightage factors assigned to the respective variables depending up on their relative significance.

The CVI values thus obtained ranged from 15 to 57. The lower range of CVI values indicate low-risk, followed by moderate-risk, high-risk and finally the upper range of values indicating the coast at very high-risk level. Accordingly, the coastal risk level map for the AP coast is generated by

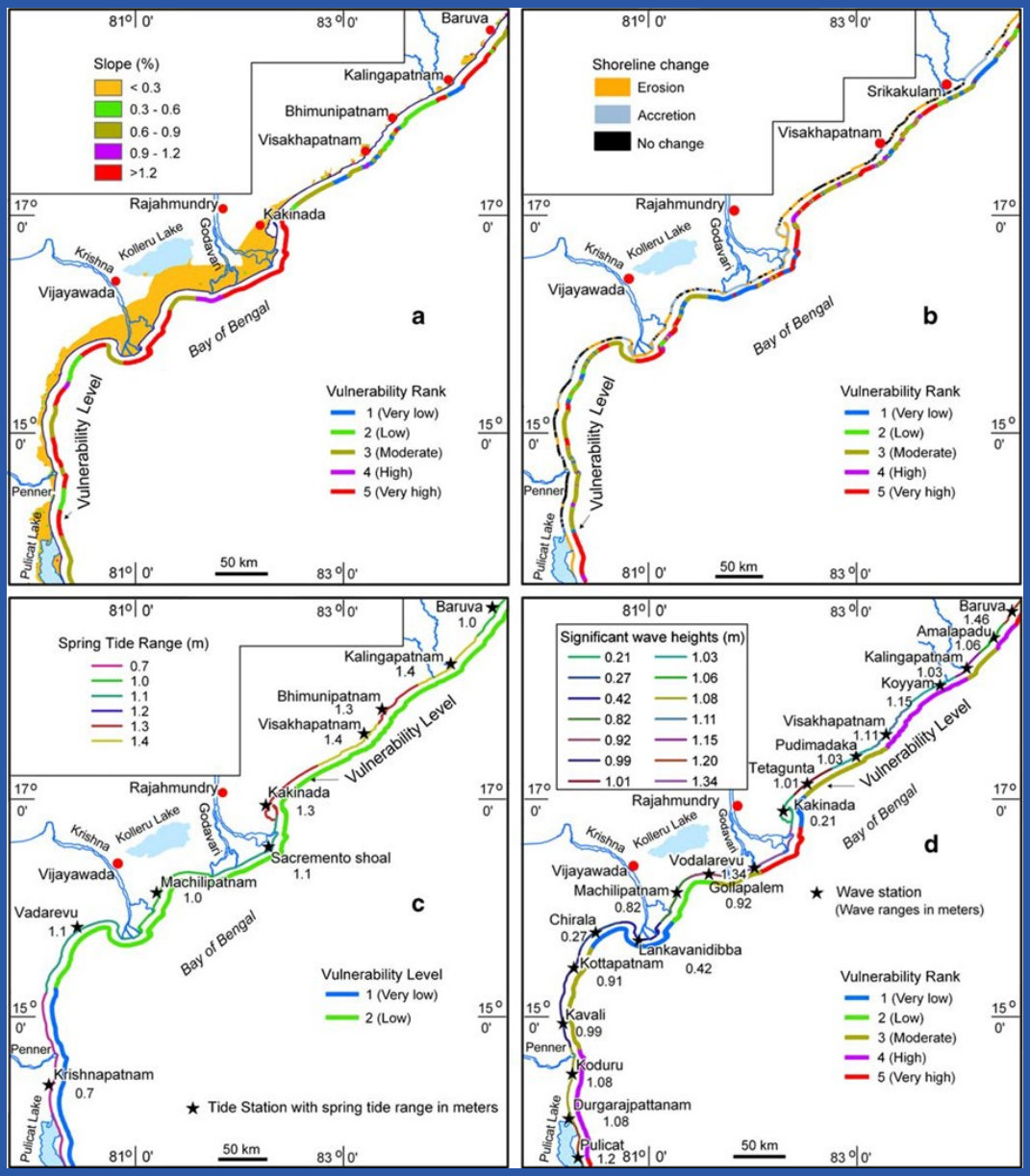

Figure 2: Map showing the four physical variables of a coastal slope, b coastal change during the 16-year period between 1990 and 2006, c mean spring-tide range, and d significant wave heights along the AP coast.

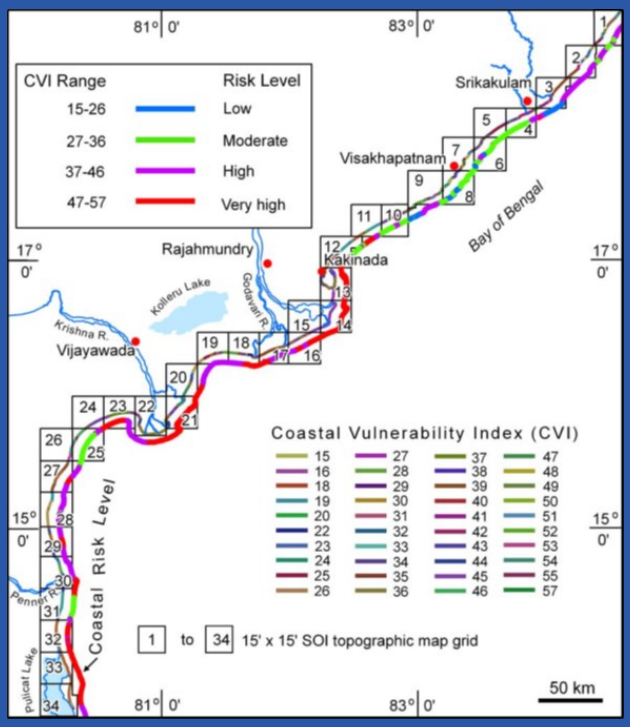

Figure 3: Coastal vulnerability index (CVI) and risk levels of AP coast. The thick colored parallel line all along the coast shows the risk levels of the coast based on the categorization of CVI values into four risk classes.

grouping various coastal segments into the four risk classes (Fig. 3). We tested these methods. The CVI values when divided into four equal parts, only the rocky coasts along the AP coast have fallen into the low risk coasts.

Development of Integrated Coastal Vulnerability Index (ICVI) for south Gujarat coast (Mahapatra et al., 2015)

South Gujarat coast is comparatively uniform and is broken by few indentations. The main coastal features are large intertidal flat, sandy beach, and sheet rock exposure in the intertidal area. Mangroves vegetation is found along the estuaries of the Auranga and the Damanganga. Numerous small tidal creeks are also found along the study area. South of Auranga estuary, the coast is rocky. The main rivers are Kolak, Damanganga, Par, Varoli, and Auranga. The study area falls under Sub-humid climate zone with annual rainfall as high as 2,000 mm. The coastline of the study area has both wave-dominated coast and tide-dominated coast.

Integrated coastal vulnerability index is developed for south Gujarat coast based on integration of physical and socioeconomic variables. Here five physical variables, namely coastal slope, Coastal landforms/features, Shoreline change rate, Mean spring tidal range, and Significant wave height, are used for the calculation of the physical vulnerability index (PVI), whereas four variables such as population density of adjacent coastal villages, land use/land cover, proximity to road network and settlement are used to assess the social vulnerability index (SVI). The weightage of PVI and SVI are then calculated using the analytical hierarchical process (AHP) method (Forman and Goss 2001). An integrated coastal vulnerability index (ICVI) has been calculated by combining PVI and SVI. The entire study area is divided into five vulnerability ranking classes—very low, low, moderate, high, and very high. The vulnerability ranking layer for physical and socio-economic variables are shown in figure 4 (A and B).

The weightage of PVI and SVI is computed using an Analytical Hierarchical Procedure (AHP) where pairwise comparison is carried out for all the factors considered, and the matrix is completed using scores based on their relative importance. Considering

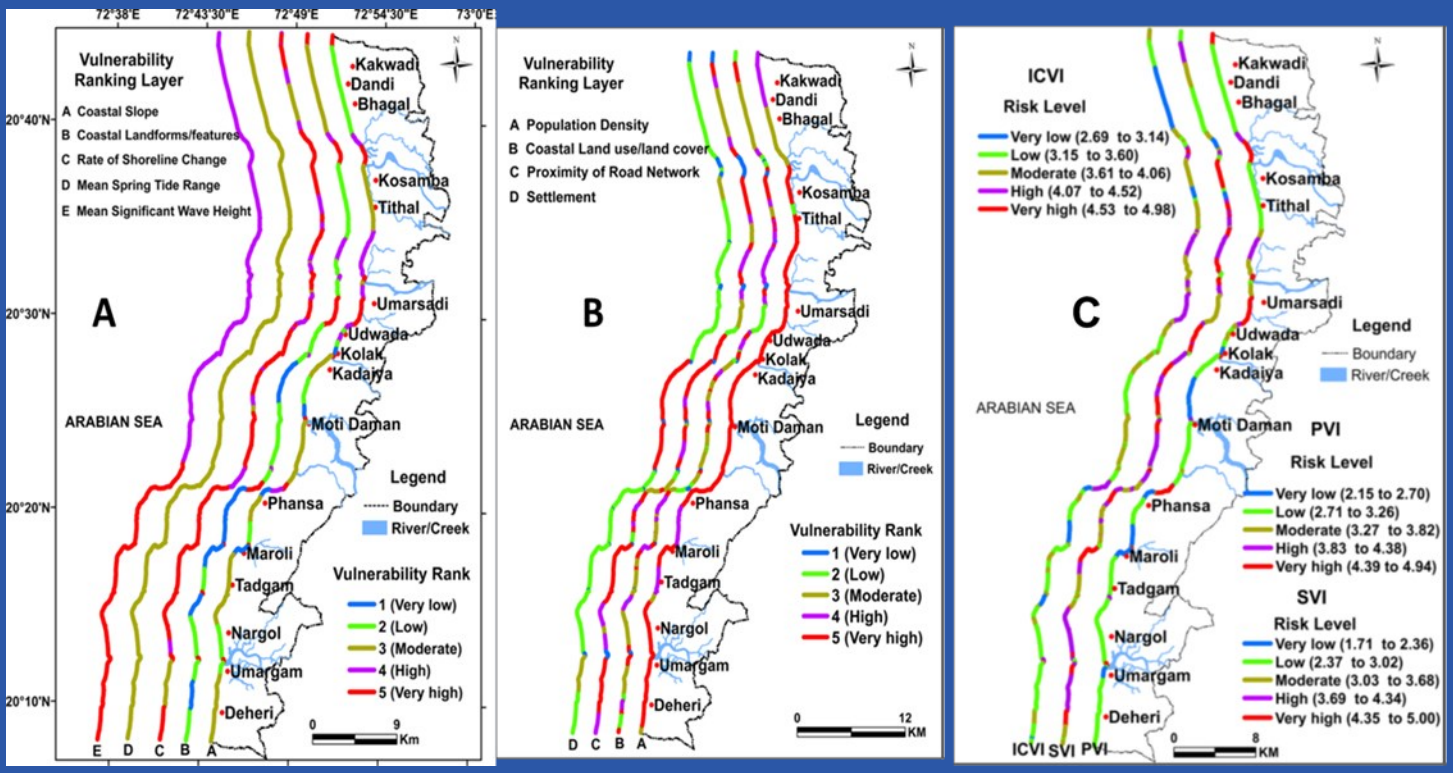

Figure 4: Vulnerability ranking layer of A) physical and B) socioeconomic variables C) Integrated coastal vulnerability index

that both physical and socioeconomic factors have equal contribution in coastal vulnerability equation 2 is used to compute the Integrated Coastal Vulnerability Index (ICVI).

ICVI = (PVI+SVI)/2

The calculated integrated vulnerability index is shown in figure 4(C).

Development of Total Vulnerability Index (TVI) for Saurashtra coast Gujarat (Mahapatra et al., 2017)

Vulnerability is a function of the character, magnitude, and rate of climate change and variation to which a system is exposed, its sensitivity, and its adaptive capacity. Hence, vulnerability is a function of: (1) the degree of exposure (E) of the system to climate variation, (2) the sensitivity (S) of the system to change in climate (the degree to which the system is affected, either adversely or beneficially, by climate related stimuli), and (3) its adaptive capacity (A) (the ability of the system to adjust to climate change, including climate variability and extremes or the degree to which adjustments in practices, processes, or structures can moderate the potential for damage). In the above definition, a system will be called highly vulnerable if it is highly exposed/ sensitive or has the potential to getting impacts due to modest change in climate and its inability to adaptation.

Exposure of a taluka can be approximated by variables linked to the storm impact and to the physical features of the taluka (Das 2012). Such variables are coastal length, low-lying area, built-up area, agricultural land, and population density. These variables increase the exposure to storm damage; hence, the more values of the above variable increase vulnerability. On the other hand, sand dune, rocky/cliffy coast,

and mangroves reduce exposure as it protects storm water to getting inundated coastal area and hence it reduces the vulnerability. The sensitivity of taluka is estimated by demographic variables such as number of population below 6 years, number of household, percentage of marginal worker, percentage of scheduled cast and scheduled tribes because of their nature of asset holding, the nature of their livelihood. The Adaptive capacity is assessed by economic well-being (presence of infrastructure such as rail, road), and population characteristics of the taluka such as percentage of literate people. The TVI is assessed using the following equation

$$TVI = (EI \times SI/AI)^{1/2}$$

where EI, SI and AI are the Exposure Index, Sensitive Index and Adaptive Capacity Index respectively. The estimated EI, SI, AI and TVI is shown in figure 5.

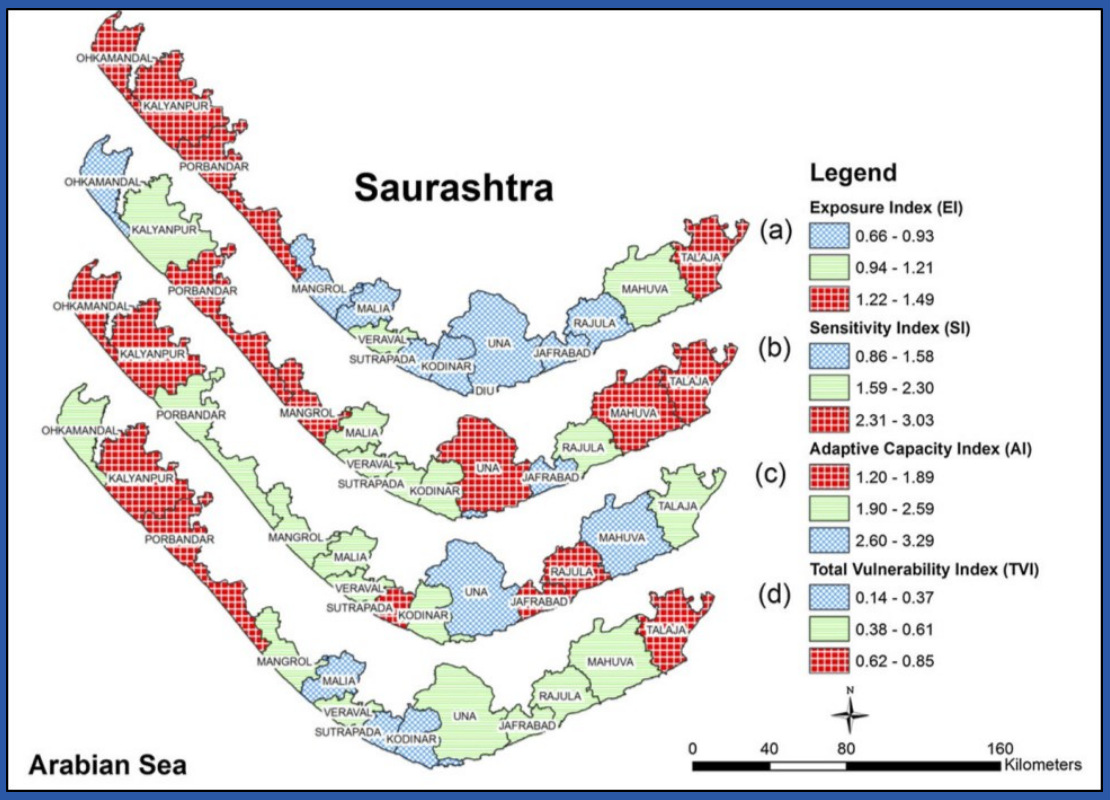

Figure 5: Vulnerability-to-storm surges assessment results in the coastal talukas of Saurashtra coast, Gujarat. Taluka-wise vulnerability map prepared from (a) Exposure Index, (b) Sensitivity Index, (c) Adaptive Capacity Index, and (d) Total Vulnerability

Potential Fishing Zone (PFZ) forecasting

R K SARANGI[1] and M JISHAD[2]
[1]MED/BPSG/EPSA, [2]OSD/GHCAG/EPSA, Space Applications Centre (ISRO), Ahmedabad
sarangi@sac.isro.gov.in

Introduction

More than 30% of India's population lives along its more than 7500 km long coastline. Fishing is a major economic activity and India is the third largest producer of fish and second largest producer of inland fish. Locating and catching fish is always a challenging task. India's scientists dealing with marine sciences, remote sensing and fishery science have collaborated to develop a technique to use the remotely sensed datasets to identify the locations of fish aggregation. The Potential Fishing Zone (PFZ) as a proxy to potential shoals of fish aggregation will benefit the fishing community to reduce the time and effort spent in searching the shoals of fish, thus improving the profitability and hence, the socio-economic status.

Trends in PFZ monitoring using satellite datasets

Applications in fisheries by remote sensing lie mostly in measuring characteristics of the physical and biological environment at the sea surface. The first application of satellite remote sensing in fisheries advisory in the US was in 1971 (Laurs, 1993). This application has had a tremendous impact on the efficiency of American tuna fleets, often reducing search times by 25% to 40% (Simpson 1992). These technologies applied to fisheries, still continue to expand and it included the Coastal Zone Color Scanner (CZCS), and the modern SeaWIFS, MODIS and Oceansat satellites, which give a synoptic view on the chlorophyll distribution in the oceans, and also the NOAA-AVHRR and MODIS satellites which are used to map sea surface temperature in a short time. These oceanographic features have been successfully mapped in near real time. In addition, phenomena such as upwelling areas, ocean colour and the presence of large amounts of chlorophyll in the water have been found as indicators of areas of fish stock congregations and fish stocks migration (Mansor et al. 2001). Satellite data from the Indian satellite IRS-P4 (Oceansat-1) ocean colour monitor (OCM) sensor, in combination with SST data are used to generate potential fishing zone (PFZ) advisories. These advisories have helped artisanal fishers reduce search time by up to 70% and have increased significantly the catch per unit effort (Solanki et al., 2003).

Thermal gradient has been included in some studies as an indicator of thermal fronts and upwelling areas, which are highly productive areas that sustain fish populations (Fernández and Pingree 1996, Olson et al. 1994, Polovina 1997). Satellite-derived chlorophyll concentrations and sea surface temperature (SST) has been traditionally used widely across the world for the identification and mapping of PFZ, the technique was developed around 2000 and the technology has been transferred to INOIS, Hyderabad for operational forecast generation. Ocean thermal fronts are the areas which are well known for upwelling and for having high chlorophyll contents (Owen, 1981; Reese et al., 2011). Hence identifying thermal fronts becomes one of the crucial components in PFZ algorithm and has been used in PFZ monitoring since long (Ardianto et al., 2017; Nayak et al., 2003; Solanki et al., 2003). The cloud cover mostly contaminates the satellite data for SST and chlorophyll. Continuous availability of satellite-based high-resolution SST and chlorophyll is therefore a major challenge, especially in the BoB, which is cloudy almost throughout the year (Zuidema, 2003) and methodology developed to have PFZ maps and forecasts during cloudy conditions (Jishad et al, 2019) and has been validated in Bay of Bengal water with catch data obtained from Fishery Survey of India (FSI). Hence it becomes quite essential to explore additional parameters from satellite and identify some features that are secondary in the formation of PFZ, for eg., mesoscale eddies, has a significant role in modulating the distribution chlorophyll and nutrient cycling in the ocean (Mahadevan, 2014; Singh et al., 2015) and upwelling zones. Other ocean parameters such as location and evolution of frontal boundaries, upwelling zones, currents, eddies, etc., are important in defining marine fish habitats (Balaguru et al., 2014). Hence, proper utilization of all these ocean features is essential for the efficient monitoring of PFZ.

Methodology used for PFZ modelling and forecasting

This methodology incorporates all the suitable ocean parameters from satellites that are linked to the production and possible availability of fishing schools and shoals in the ocean region. The ocean parameters include high chlorophyll concentration features, thermal fronts based on SST gradients, locations of cyclonic and anti-cyclonic eddies, relative wind (wind and current vectors) based Ekman fronts. The novel part of the methodology lies in the tracking of PFZ by linking the propaga-

tion of thermal fronts with respect to the water mass transport connected to Ekman pumping and upwelling processes.

The feature based PFZ monitoring and prediction forecasting has been generated using near real time satellite dataset with limited validation (Jishad et al, 2019). The new methodology has been used to predict PFZ locations for t_0^{th} day. The oceanic eddies are identified and tracked (Chelton et al., 2011) and identified cold and warm core eddies. The SST gradient and thermal fronts are generated for the t_0 day from MODIS SST. The 3-day running average (t_0-2, t_0-1 and t_0) chlorophyll data for MODIS-aqua has been used as background. The more weightage is given to the regions encompassing high chlorophyll concentration, thermal fronts and cold core eddies. The possible propagation of PFZ regions has been identified using relative wind (ocean surface wind field minus surface current) field. The relative wind fields and the corresponding Ekman transport for the day t_0 have been obtained. Chlorophyll image is overlaid on the representative eddies, SST

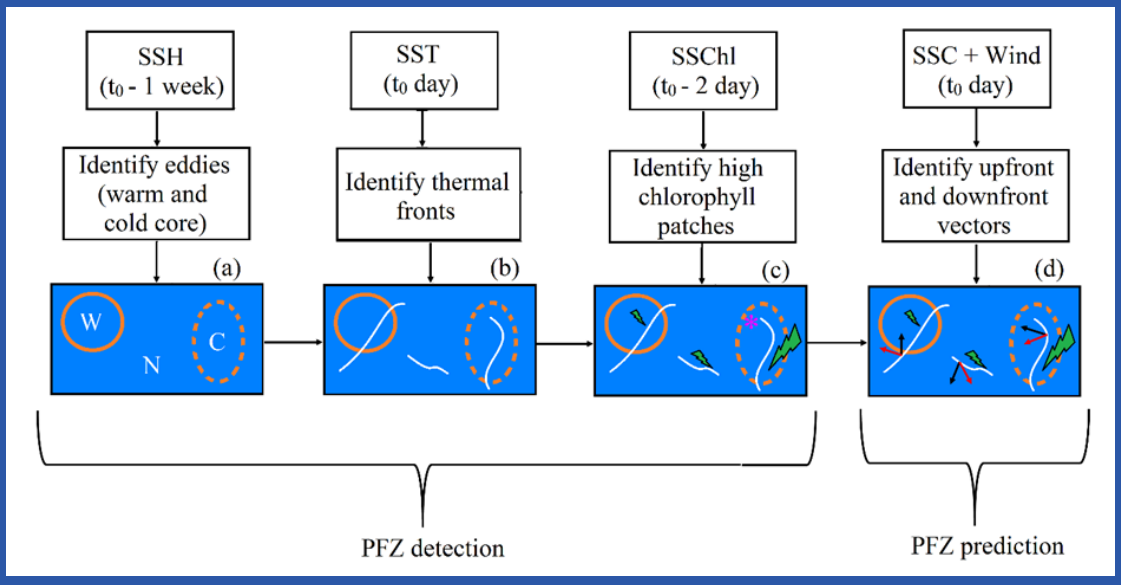

*Figure 1: Potential fishing zone identification: A comprehensive schematic from satellite-based multi-sensor observations. Thermal fronts, eddies and chlorophyll concentration patches are shown as white lines, orange circles and green patches respectively. W: Warm core Eddy, C: Cold core Eddy, N: No eddies. Black and red vectors represent Ekman transport and frontal direction. * in (c) represents the preferable ocean conditions for identifying PFZ*

Dataset used

Various oceanic and atmospheric parameters from different satellites are processed for understanding the relation between fish catch locations and ocean parameters. A near real time forecast has been provided using satellite data for Tamilandu coast. The forecast has been generated using Chlorophyll and SST data from MODIS (with delay of one day), ocean surface winds from ISRO launched scatterometer, SCATSAT-1 (6.25km with a delay of one day), Hycom model current data of 9.1 km resolution and Sea surface height (SSH) (25km) by AVISO. In order to reduce the cloud coverage in chlorophyll data, the daily data has been averaged for 3-days and composites have been generated.

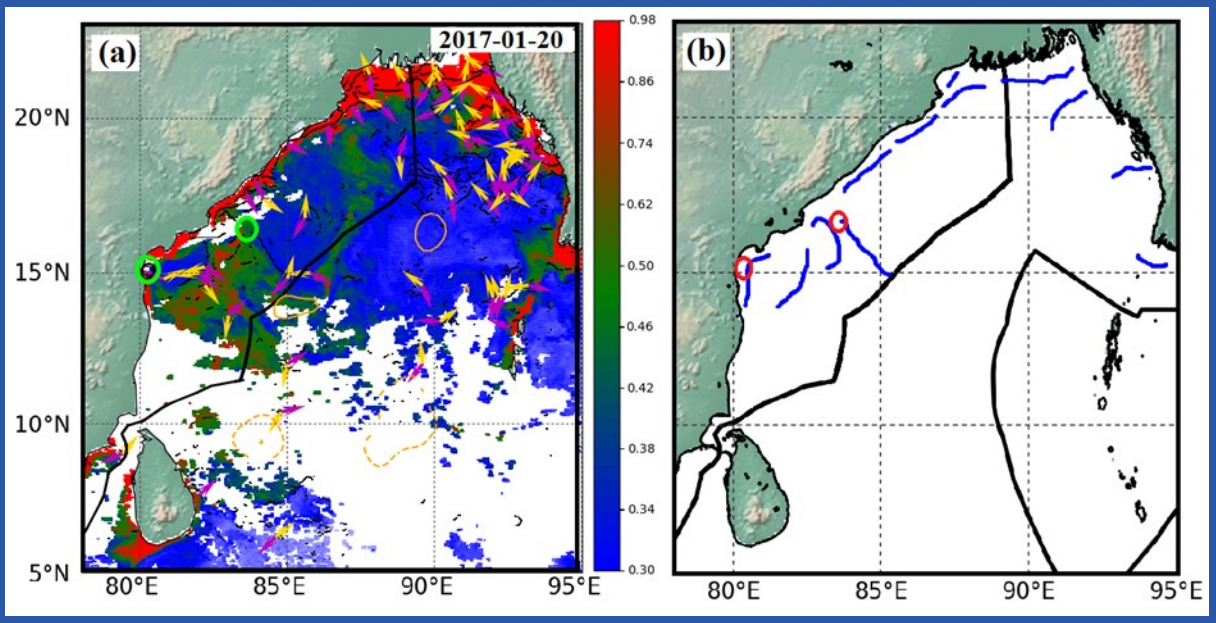

Figure 2: (a) An example showing conditions considered for the generation of PFZ maps. CHL (mg/m^3) is shown as shaded plot, which is overlaid by thermal fronts (black lines), cyclonic (dashed yellow contour) and anticyclonic (closed yellow contour) eddies, Ekman transport (yellow vector) and frontal direction (pink vector). The thick black line shows EEZ boundary. (b) The identified PFZ locations are overlaid with the in-situ fish catch data locations as red circles. The thick black line shows EEZ boundary.

Validation of PFZ

To validate the authenticity of the feature based PFZ forecast approach, the hind cast data for the last 3-years for the offshore and coastal waters have been utilized and interpreted. The fish catch data obtained from FSI, Mumbai for the years 2016, 2017 and 2018, categorizing both long line based hooks (Drishti Vessel) and bottom trawl gear (Samudrika Vessel) sources have been utilized for validation of the feature based PFZ approach. The CPUE and hook rates data obtained from FSI have been utilized in this study. The CPUE is calculated as the total fish catch in respective number of hours during a single haul operation during the trip using a single boat (total fish catch/number of hours). This is linked to the trawl net operations. In our study, CPUE is measured using trawl net

along coastal waters off Tamilnadu and AP coasts. The fish catch weight by single boat observation have been in few hundreds of kilograms as maximum catch for couple of hour trawl net operation. For the long lines operation in the deeper waters, the hook rate is taken account and linked to the total catch. In a single longline, there used to be 90 hooking chains and in each chain there used to be 7 hooks in the gap of about 1 meter as the mono-filament hook line. So, the hook rate is calculated as accordingly; Hook rate= Number of fish *100/ total number of hooks.

The near real time forecast has been provided to collaborating agencies (CAs). The validation has been carried out for the coastal and offshore waters in BoB off Tamilnadu and AP coast with the datasets obtained from FSI. The hook rate categories (1.0-3.0 and >3.0) and CPUE categories (50-100 and >100) data points during the respective date and locations during 2016-2018 have been analyzed and interpreted with PFZ maps and individual oceanographic parameters. Figure 3a shows the comprehensive view of the above-described steps, which include the use of eddies, SST fronts, Ekman transport vectors, upwelling zones and chlorophyll images to detect and forecast PFZ for 8th march 2019. A final PFZ map corresponding to figure 3a is shown in figure 3b. PFZ locations are marked in blue colours to demarcate the regions of high probability for the fish catch. The operational forecast given by ESSO-INCOIS for the corresponding date is shown in figure 3c. The yellow lines in the figure 3c show the forecasted PFZ locations. One can see from the figure that two locations are matching with operational forecast given by INCOIS. The PFZ validation campaign was conducted at off Chennai (Location1, figure 3b) and

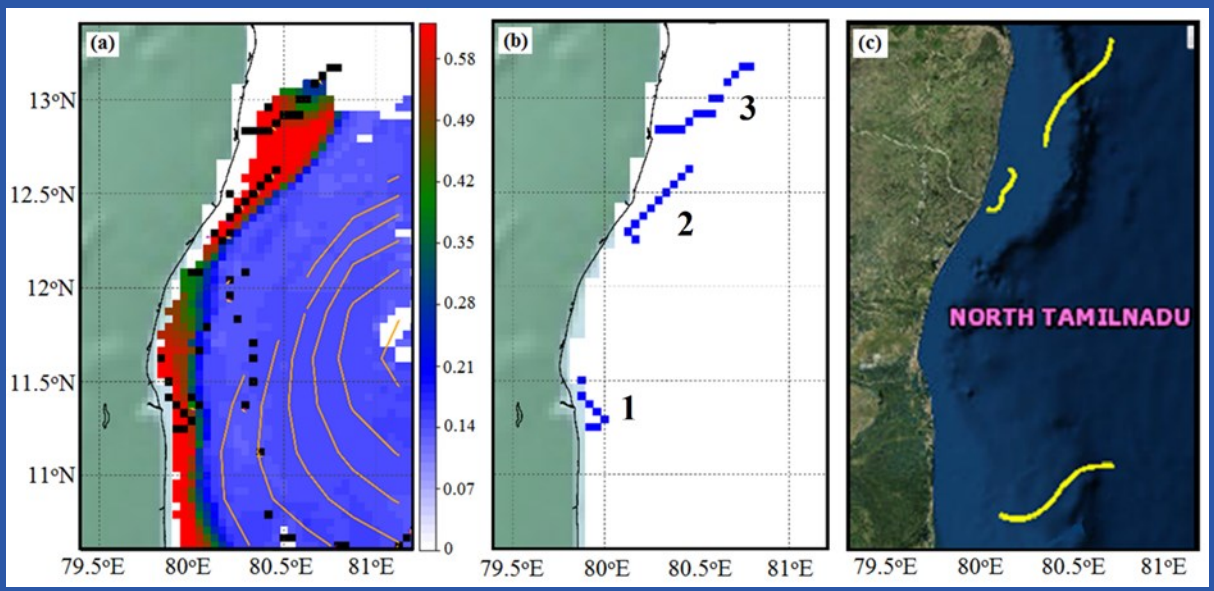

Figure 3: (a) Comprehensive image of the input parameters such as eddies, SST fronts, Ekman transport vectors, upwelling zones and chlorophyll images to detect and forecast PFZ (b) Final PFZ map and (c) ESSO-INCOIS operational forecast for 08-03-2019.

the catch was very promising (Fig. 4) with the performance of the modified methodology.

Summary and conclusion

As mentioned in the above sections, high concentrations of chlorophyll along the thermal front and/or cold core eddy and/or upwelling zones are considered as the regions of possible fish catch. The PFZ maps have been generated using the feature based algorithm and have been displayed for the catch data dates for both the coastal (bottom trawl operation) and offshore (long line operation) locations. The high chlorophyll patches, SST fronts, eddies, Ekman transport vectors, upwelling zones, etc. have been identified and linked to the persistence of high productive features in the fish catch locations in the Bay of Bengal.

After generating PFZ maps, next step was the validation of the identified PFZ. It is a mandatory step in every technique before its implementation and here PFZ validation means the process of confirming that the results are matching with in situ fish catch data obtained from a fishing vessels. It is difficult to give accurate PFZ advisories over some fish locations due to cloud cover. PFZ validation campaigns have been conducted with help of Collaborating Agency [Fishery Survey of India] for 2016 to 2018 datasets. The catches covered a broader range, from few kilograms to hundreds of kilograms for trawl net fishing using a single boat and which is in thousands of kilograms in case of offshore/longline fishing. Hence the hook rate approach has been adapted for the offshore catch validation.

Figure 4: Total catch from Odisha Coast and Tamilnadu coast during PFZ validation campaigns.

Further Reading

- Allen J C, et al., (2006). J Coast Res 22:511–529 doi:10.2112/03-0108.1.
- Ardianto, R., et al., (2017). IOP Conference Series: Earth and Environmental Science, pp. 012081.
- Balaguru, B., et al., (2014). The International Archives of Photogrammetry, Remote Sensing and Spatial Information Sciences, 40(8): 1017.
- Banse, K., (1987). Deep-Sea Research, Vol. 34, 5/6, 713 – 723.
- Bhattacharya, B. K., et al., (2013), International Journal of Remote Sensing, 34(20), pp. 7069-7090.
- Bhatti, H., et al., (2018). Current Science (00113891) 114 (12).
- Caraux, D., (1983). Rem. Sens. Environ., 13, 239-249.
- Chelton, D.B., et al., (2011). Progress in Oceanography, 91(2): 167-216.
- Courtland R, (2008). Nature 453:432– 433
- Fernández, E., et al., (1996). Deep-Sea Res. 43(9): 1369.
- Fu, L.-L., et al., (2001). , 463 pp., Academic, San Diego, Calif.
- Gaina, C., et al., (2007). Geophysical Journal International, 170,151–169.
- Hansen J, et al., (2006). Proc Natl Acad Sci USA 103:14288–14293 doi:10.1073/pnas.0606291103
- Hwang, C., et al., (2002). J. Geod. 76, pp. 407-418.
- IOCCG Report Number 3, 2000, Remote sensing of ocean colour in coastal, and other optically-complex waters.
- IPCC., (2007). Intergovernmental panel on climate change. climate change 2007: the physical science basis. Summary for policymakers.
- Jishad, M, et al., (2019). Jrnl of Operational Oceanography, [doi.org/10.1080/1755876X.2019.1658566].
- Knutson TR, et al., (2010). Nat Geosci 3(3):157–163. doi:10.1038/ngeo779.
- Krishna, K.S., et al., (2009). J. geophys. Res., 114,B03102, doi:10.1029/2008JB005808.
- Laurs RM. (1993). Lecture notes of International workshop on application of satellite remote sensing for identifying and forecasting potential fishing zones in developing countries.
- Lenoir J, et al.,(2008). Scientist 320:1768–1771.
- Mahadevan, A., (2014). Nature, 506(7487): 168.
- Mahapatra M, et al., (2015). Natural Hazard, 76: 139-159.
- Mahapatra M, et al., (2017). Nat Hazards. 86:821–831
- Majumdar, T.J., et al., (1998). Report no. SAC/RSAG/TR-01/98, p 40.
- Majumdar, T.J., et al., (2004). Report no. SAC/RESIPA/MWRG/ESHD/TR-21/2004, p46.
- Mansor, S., et al., (2001). 5-9 November 2001. Asian Association on Remote Sensing (AARS). Singapore.
- Mathew, S., (2006). Berlin, Heidelberg: Springer-Verlag.
- Mishra, A.., et al., (2018). Tectonophysics, 744, 82-92,
- Muthusankar, G., et al., (2017). Nat Hazards, 85:637–647.
- Nayak, S. R., et al., (1991). Technical Note, IRS-UP/SAC/MCE/TN/32/91 (SAC, Ahmedabad), 63 p.
- Nayak, S., et al., (2003). Utilization of IRS-P4 Ocean colour data for potential fishing zone—a cost benefit analysis.
- NCSCM, (2015). NCSCM Technical Report Series, 23 B.
- Nicholls, R. J., et al., (2010). Science, 2010, 328, 1517.
- Olson, D. B., et al., (1994). Oceanography 7:52–60.
- Papa et al (2010), J Geophys Res, doi:10.1029/2009JD012674
- Peduzzi P, et al., (2012). Nat Clim Change 2(4):289–294. doi:10.1038/nclimate1410
- Pendleton EA, et al., (2004). USGS Open File Report 2004-1064.
- Platt, T., et al., (1991). J. Geophys. Res., 96C: 15,147 -15,159.
- Polovina, J.J. (1997). Local-scale swordfish fisheries oceanography. In: Second international Pacific Swordfish symposium, Hawaii, March 3-6.
- Rajawat, A. S., et al., (2015). Current Science, 109 (2), 347–353.
- Rajawat, A. S., et al., (2015). Curr. Sci., 109(2), 347–353.
- Rao, N.P. et al., (2009). Journal of Coast Conservation. DOI 10.1007/s11852-009-0042-2.
- Ratheesh R., et al., (2018). Ocean & Coastal Management 156, 239-248.
- Reese, D.C., et al., (2011). ICES Journal of Marine Science, 68(9): 1865-1874.
- Remya, G., et al., (2011). IEEE Geosciences Remote Sensing Letters, 8(2), pp. 354-358.
- Safari, B. et al., (2010). Renewable Energy, 35, pp. 2871-2880.
- Sandwell, D.T., et al., (2014). Science 346, 65.http://dx.doi.org/10.1126/science.1258213
- Santos M, et al., (2013). J Coast Res 65(SI):826–831.
- Sathyendranath, S., et al., (1991). Nature, 349:54-56, 1991.
- Simpson, J.J. (1992). A publication of the California Sea Grant College, Report No. T-CSGCP-025.
- Singh, A., et al., (2015). Journal of Sea Research, 97: 5-13.
- Small C, et al., (2003). J Coast Res 19(3):584–599.
- Solanki, H. et al., (2003). International Journal of Remote Sensing, 24(18): 3691-3699.
- Sowmya K., et al., (2019). International Journal of Sediment Research 34: 335–344.
- Sreejith K.M., et al., (2015). Geophysical Research Letters, 42, doi: 10.1002/2014GL062993.
- Sreejith K.M., et al., (2016). Journal of Asian Earth Sciences, 131, 1–11, http://dx.doi.org/10.1016/j.jseaes.2016.09.002.
- Sreejith, K. M., et al., (2019). Journal of Earth System Science, 28:157;
- Sreejith, K.M., et al., (2011). Journal of Earth System Science, 120, 605-615.
- Sreejith, K.M., et al., (2013). Journal of Asian Earth Sciences. 62, 616–626.
- Srinivasa Rao, et al., (2016). Geophysical Journal International, 206, 675-695.
- Surisetty V.V. Arun Kumar et al., (2016). Current Science, 111(5), pp. 836-842.
- Watts, A.B., (2001). pp. 458, Cambridge University Press, UK.
- Wernand, M.R., et al., (2013). PLoS ONE, 8(6): e63766. Doi:10.1371/journal.pone.0063766.
- Yan, Q., et al., (2010). Acta Geoscientica Sinica, 31 (5), pp. 759-767.
- Zibordi, G., et al., (1990). Remote sensing of the environment, Vol. 34, pp. 49 – 54.

Interesting News about Oceans

Enter the twilight zone: Scientists dive into the ocean's mysterious middle

(Source: https://www.nature.com/articles/d41586-020-00520-8)

Ocean twilight zone is a stratum of water that extends all around the globe (layer extending from 200 to 1,000 meters deep in oceans). According to a news article published in Nature, attempts are being made by scientists to explore the twilight zone of oceans. The zone begins where the photosynthesis process shuts up entirely and reaches down where there is complete extinction of light. The region is swarmed up with life ranging from microscopic to world's largest species. There are many marine creatures that inhabit in ocean's twilight zone and still remains unidentified.

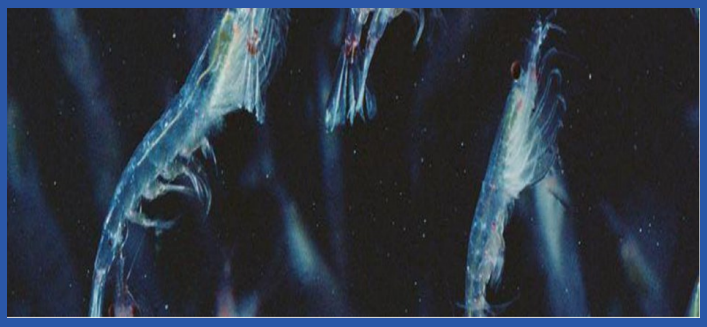

Figure: Twilight zone inhabited by wide range of invertebrate species may represent a major source of protein. (Credit Flip Nicklin/ NPL).

Predatory animals like whales and sharks try to hunt in this region of water in search of food. Humans are also keeping eye on how to venture in this band of water. Scientists fear that climate change and overfishing will have an impact on this zone and could even affect the marine food web.

Record-Setting Ocean Warmth Continued in 2019

(Source: Cheng et al., Advances in Atmospheric Sciences, Vol. 37, February 2020, 137–142)

Earth's ocean recorded the warmest temperature in 2019 which is considered to be maximum in the human history recorded so far. Reason for increase in temperature is the global warming itself. Ocean heat content values quantify the rate of global warming showing the record setting ocean warmth in 2019 when compared with the average year values (1981-2010).

According to Lijing Cheng,

"*This measured ocean warming is irrefutable and is further proof of global warming. There are no reasonable alternatives aside from the human emissions of heat trapping gases to explain this heating*".

Upcoming Conferences 2020

- ISPRS TC V- UASG-2020
- Second International Conference on Unmanned Aerial Systems-2020, Greater Noida, India, 31st Oct - 02 Nov 2020
- SPIE Remote Sensing, Edinburgh International Conference Centre, Edinburgh, United Kingdom, 21 - 24 September 2020
- 3rd International Conference on Renewable Energy and Resources, Vancouver, Canada, August 24-25, 2020
- 9th World Conference on Earth & Environmental Science, Edinburgh, Scotland, August 24-25, 2020
- 11th World Climate Change Conference, Valencia, Spain, September 09-10, 2020
- IEEE International India Geoscience and Remote Sensing Symposium 2020

  "Remote Sensing coming of the age in Global Community", Ahmedabad, Gujarat, India, 1-5 December 2020
- IEEE International Geoscience and Remote Sensing Symposium, Waikoloa, Hawaii, USA, July 19 – 24, 2020
- Pan Ocean Remote Sensing Conference, Malaysia, 20 - 22 Sep 2020
- 6th International Conference on GIS and Remote Sensing 2020, Barcelona, Spain, 23-24 Nov 2020
- Geosmart India 2020, Hyderabad, India, 6-8 October 2020
- IOCCG-25 Committee meeting, Tokyo, Japan, March 27-29, 2020
- SPIE, Space, Satellites and Sustainability, Edinburgh, United Kingdom, September, 19-23, 2020
- Oceans from Space, 5th edition, Venice, Italy, October 12-16, 2020
- PORSEC 2020, 15th PAN ocean remote sensing conference, Malaysia, Sept 15-22, 2020
- International Conference On Aquaculture and Marine Biology

  THEME: New Advancements in Aquaculture & Marine Biology, Kanyakumari, India, September 18 - 19, 2020

SIGNATURES

ISRS-AC Executive Council 2020-2022

Chairman	**Shri Rajeev Jyoti**, Space Applications Centre, ISRO, Ahmedabad—380015 rajeevjyoti@sac.isro.gov.in
Vice-Chairman	**Dr. Shital H. Shukla** , Gujarat University, Ahmedabad—380009 shitalshukla25@yahoo.co.in
Secretary	**Dr. D. Ram Rajak** , Space Applications Centre, ISRO, Ahmedabad—380015 rajakdr@sac.isro.gov.in
Joint Secretary	**Dr. Alpana Shukla,** M G Science Institute, Ahmedabad—380009 alpana.botany@gmail.com
Treasurer	**Shri Ritesh Agrawal**, Space Applications Centre, ISRO, Ahmedabad—380015 ritesh_agrawal@sac.isro.gov.in
Members	**Shri K. P. Bharucha**, Retd. Scientist, Space Applications Centre, ISRO, Ahmedabad—380015 kishorbharucha@gmail.com
	Ms. Akriti Kulshrestha, Space Applications Centre, ISRO, Ahmedabad—380015 akriti.kulshrestha@sac.isro.gov.in
	Ms. Samarpita Sarkar, Space Applications Centre, ISRO, Ahmedabad—380015 samarpita@sac.isro.gov.in
	Dr. Satyendra M. Bhandari, Retd. Scientist, Space Applications Centre, ISRO, Ahmedabad—380015 space.scientist@gmail.com
	Dr. P. S. Thakker, Retd. Scientist, Space Applications Centre, ISRO, Ahmedabad—380015 thakkerps@gmail.com
Ex-Officio Chairman	**Dr. Raj Kumar,** Space Applications Centre, ISRO, Ahmedabad—380015 rksharma@sac.isro.gov.in

EDITORIAL TEAM

Dr. Rashmi Sharma

rashmi@sac.isro.gov.in

Dr. Bipasha Paul Shukla

bipasha@sac.isro.gov.in

Dr. Rimjhim Bhatnagar Singh

rimjhim@sac.isro.gov.in

Dr. Surisetty V.V. Arun Kumar

arunkumar@sac.isro.gov.in

Ms. Nimisha Singh

nimisha@sac.isro.gov.in

Contacts

Dr. Rashmi Sharma
Editor
"Signatures "
ISRS-AC Newsletter
Room #6056, Space Applications Centre,
Bopal Campus
Ahmedabad, Gujarat
Email: rashmi@sac.isro.gov.in

Dr. A.S. Rajawat
Secretary, ISRS-AC
Room #4018, Space Applications Centre,
Ahmedabad, Gujarat
Email: asrajawat@sac.isro.gov.in